

A stochastic partial transport model for mixed-size sediment: Application to assessment of fractional mobility

Fu-Chun Wu

Department of Bioenvironmental Systems Engineering and Hydrotech Research Institute, National Taiwan University, Taipei, Taiwan

Kuo-Hsin Yang

Department of Bioenvironmental Systems Engineering, National Taiwan University, Taipei, Taiwan

Received 12 April 2003; revised 30 November 2003; accepted 20 January 2004; published 3 April 2004.

[1] In this study we incorporate the existing concept of fractional mobility into a stochastic framework for modeling the partial transport of mixed-size sediment. The model predicts the fractional transport rates with parameters such as the long-run moving probability, mean particle velocity, and fractional mobility, all varying with the dimensionless effective shear stress. Movement of bed load particles is treated as a random combination of single-step motions described by the pseudo four-state continuous-time Markov process whose long-run moving probability can be evaluated with the instantaneous entrainment probability and ratio of mean single-step holding time. A most updated version of entrainment probability taking into account both the rolling and lifting modes is adopted; the ratio of mean holding time is determined with a physically based relation derived experimentally. Two types of experiments are performed in this study: the colored bed experiments are carried out to observe the fractional mobility and partial transport; the plain bed experiments are conducted to observe the single-step bed load motions and mean particle velocity. The proposed model is widely tested with laboratory and field data pertaining to both partial and full transport conditions, and reasonably good agreement between the predicted and observed results is demonstrated. The model is then applied to evaluate the fractional mobility and explore the influence of sand content. The results reveal that the relation between fractional mobility and dimensionless effective shear stress is well approximated by the cumulative lognormal distribution, with its mean and standard deviation linearly decreasing with sand content for the range <0.34 . The results imply that the existence of fine-grained sand in the gravel-sand mixture is favorable to the mobilization of sediment. At higher sand content the condition of partial transport exists within a narrower range of flows such that full transport is easier to achieve. The present study is the first to investigate the effect of sand content on the fractional mobility, thus providing new insights into the process of partial transport. *INDEX TERMS:* 1815 Hydrology: Erosion and sedimentation; 1824 Hydrology: Geomorphology (1625); 1869 Hydrology: Stochastic processes; *KEYWORDS:* stochastic model, partial transport, mixed-size sediment, fractional mobility

Citation: Wu, F.-C., and K.-H. Yang (2004), A stochastic partial transport model for mixed-size sediment: Application to assessment of fractional mobility, *Water Resour. Res.*, 40, W04501, doi:10.1029/2003WR002256.

1. Introduction

[2] It is well known that the transport of sediment in gravel bed rivers is associated with a condition of partial transport over a range of flows. Within this range, some grains exposed on the bed surface are active (i.e., entrained at least once over the duration of a transport event), while the remaining are immobile [Wilcock and McArdell, 1993, 1997]. For example, a recent field study [Haschenburger and Wilcock, 2003] reported that full mobilization of surface grains is not a frequent event and the inactive regions of the bed surface typically persist from year to year. The condition

of partial transport is important for modeling the process involving grain sorting or size-selective transport, such as the bed armoring, selective deposition, downstream fining, and flushing of fine-grained sediment from gravel riverbeds [e.g., Parker and Sutherland, 1990; Paola *et al.*, 1992; Hoey and Ferguson, 1994; Wu, 2000; Wu and Chou, 2003b]. Most previous bed load models for mixed-size sediment were developed for the full transport condition (i.e., for flows beyond the limit of partial transport, or for fully mobilized sand riverbeds), some of which were based on the empirical flow-transport relations derived from the laboratory or field studies without noticing the existence of immobile surface grains. Thus applications of these models to the prediction of partially mobilized transport are indeed questionable.

[3] The partial transport model presented by *Wilcock* [1997] was the first to systematically incorporate the fractional mobility of mixed-size sediment into a quantitative framework. Although some of the model parameters (such as the fractional mobility and reference shear stress) were determined from the limited data then available, lately a series of experiments over a range of flows and sediments have been conducted and led to the modified forms of reference shear stress that incorporate the effect of sand content on the entrainment of mixed-size sediment [*Wilcock et al.*, 2001; *Wilcock and Kenworthy*, 2002; *Wilcock and Crowe*, 2003]. However, the fractional mobility was not included in their new data set, thus the effect of sand content on the fractional mobility still remains to be understood. The concept of active layer (also known as exchange, mixing, or surface layer) has been extensively adopted in modeling the transport of sediment mixtures since its first introduction [*Hirano*, 1971]. The original active layer concept is problematic in that it divided the bed into a discrete active layer and substrate, and assumed no sediment flux across the interface between active layer and substrate. This was modified by *Armanini* [1995] who proposed a continuum model of vertical exchange, which was further developed by *Parker et al.* [2000] with the introduction of a probabilistic model. Recently, *Wu and Chou* [2003b] have used a simplified active two-layer framework to simulate the interactions between surface and subsurface layers, and confirmed the operation of an upward sand flux from subsurface that has only been hypothesized before. On the other hand, *Sun and Donahue* [2000] presented a bed load model for nonuniform sediment incorporating the stochastic characteristics of sediment transport. Their model, originally developed for the fully mobilized transport, was modified to predict the partial transport by including the fractional mobility as a model parameter. However, the primary drawbacks of their model include the ambiguous use of continuous- and discrete-time Markov processes, and inconsistency involved in the definitions of the parameters. For example, their two-state model was defined by a continuous-time Markov process, but the transition probabilities they used were only suitable for the discrete-time Markov process; the entrainment probability used in their model was for the rolling mode, but their mean particle velocity was solely for the saltation mode. In addition, nearly all of their model parameters were calibrated with only the full transport data, which could potentially lead to discrepancies in the prediction of partial transport.

[4] The aim of this study is to develop a stochastic bed load model applicable to the partially mobilized transport. Stochastic methods have been shown a promising approach to modeling bed load transport [e.g., *Einstein*, 1950; *Paintal*, 1971; *Wu and Wang*, 1998; *Sun and Donahue*, 2000]. The primary distinction between the stochastic and deterministic bed load models is that the former does not need a critical shear stress (or reference shear stress) as the threshold for sediment entrainment/transport. Rather, researchers using stochastic models tend to believe the existence of a range of thresholds for incipient motion and thus employ the probability of entrainment to incorporate this uncertainty. To date, a variety of entrainment probabilities have been presented, e.g., rolling probability [*Sun and Donahue*, 2000; *Wu and Chou*, 2003a], lifting probability [*Einstein*, 1942; *Cheng and Chiew*, 1998; *Wu and Lin*, 2002], and sliding

probability [*Paintal*, 1971]. The differences between these probabilities mainly arise from the entrainment mechanism and the random components (such as turbulent fluctuations, sediment property, and bed configuration) that are considered in the mathematical formulation.

[5] In this paper we present a stochastic partial transport model based on the pseudo four-state continuous-time Markov process, eliminating the ambiguousness involved in the two-state model. The proposed model incorporates a most updated version of entrainment probability and a set of parameters derived from an assemblage of new experimental data and existing research results. The proposed model was tested with the laboratory and field data pertaining to both the partial and full transport conditions. The model was further applied to evaluate the fractional mobility using the laboratory and field data observed over a wide range of flows and sediments. The present study is the first to explore the effect of bed sand content on the fractional mobility, thus provides new insights into the process of partial transport.

2. Simplified Concept of Fractional Mobility

[6] Before we proceed to present stochastic modeling of partial bed load transport, it would be useful to introduce a simplified concept of fractional mobility. For a partially mobilized mixed-size sediment, the mobility of size fraction i , denoted as Y_i , is defined as the proportion of active grains in that fraction [*Wilcock and McArdell*, 1997]. Specifically, partial transport corresponds to a condition $0 < Y_i < 1$ for at least one size fraction i , whereas full transport means that $Y_i = 1$ for each i . Given the active proportion of each size fraction, it is possible to divide the sediment on the bed into two classes of population, i.e., one includes all the active grains and the other includes all the immobile ones. Since the former consists of all the active grains on the bed, it is hypothesized that for sufficiently long sampling time all these active grains can be collected as bed load. The proportion of fraction i in this active class (i.e., bed load), denoted as p_i , can be expressed as

$$p_i = \frac{Y_i f_i}{\sum_j Y_j f_j} \quad (1)$$

where f_i = proportion of fraction i on the bed. For equal mobility of all size fractions (i.e., $Y_j = \alpha$ for all j , e.g., $\alpha = 1$ for the fully mobilized transport), (1) would reduce to $p_i = f_i$ (given $\sum_j f_j = 1$), indicating that the ratio $p_i/f_i \rightarrow 1$ as the bed load transport approaches an equally mobilized condition, which is most likely to occur at a state of full transport. However, for unequal mobility of the mixed-size sediment, (1) can be rewritten as

$$\frac{p_i}{f_i} = \frac{Y_i}{\sum_j Y_j f_j} = \frac{Y_i}{\bar{Y}} = Y_i^* \quad (2)$$

where \bar{Y} and Y_i^* = mean mobility of sediment and relative mobility of fraction i on the bed, respectively. The quantitative relations given by (1) and (2) represent a simplified concept of fractional mobility, which is based on an assumption that all the active grains can be collected

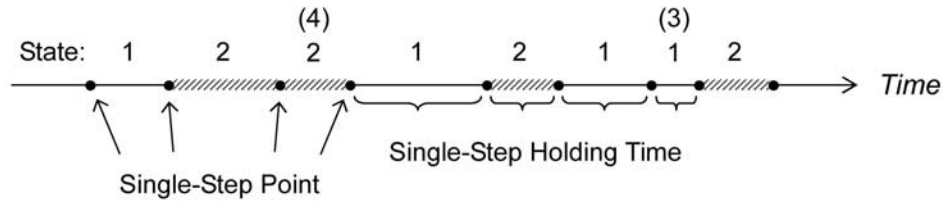


Figure 1. Time axis representation of pseudo four-state continuous-time Markov process. A single-step motion, either in state 1 or 2 (i.e., static or moving state), takes place between two consecutive single-step points.

during a transport event. However, this is not always true because some active grains only move sporadically and thus are unable to reach the sampling location. This assumption is a special case of the general partial transport condition; it is only valid for the continuous (or quasi-continuous) bed load movement.

3. Stochastic Partial Transport Model

3.1. Pseudo Four-State Continuous-Time Markov Process

[7] Many previous observations [e.g., *Einstein, 1937; Hubbell and Sayre, 1964*] have indicated that the movement of a bed load particle can be viewed as a random combination of two distinct states, i.e., static (or resting) and moving, designated as states 1 and 2, respectively. As depicted in Figure 1, the time axis is composed of many segments bounded by the single-step points. A single-step motion, either in the static or moving state, takes place between two consecutive single-step points at which the bed load particle has chances to change its motion states. For instance, in our flume studies we have frequently observed that a moving particle strikes an obstacle and ends up with two different results, i.e., the moving particle either stops, changing its state from moving to resting, or continues to move, maintaining its moving state; in the latter case no transition of state occurs. We have also seen that an initially static particle entrained by an instantaneous turbulent burst has a chance to change its state from resting to moving, but turns out to be hampered by surrounding grains and thus no transition of state occurs. These are some typical examples of the single-step point at which the transition of motion state may occur. Such a two-state stochastic process can be perfectly cast into the framework of a continuous-time Markov chain if the motion states are properly restructured as the following.

[8] According to the definition of a continuous-time Markov process, if the process leaves state m and next enters state n with a probability P_{mn} , then P_{mn} must satisfy $P_{mm} = 0$ and $\sum_n P_{mn} = 1$ for all m . If this condition were violated, i.e., $P_{mm} \neq 0$, it would become a discrete-time Markov process, which is unsuitable for modeling bed load transport due to the lack of a holding-time component. For the movement of a bed load particle as illustrated in Figure 1, two types of state transition (i.e., state transitions $1 \rightarrow 1$ and $2 \rightarrow 2$) contradict the definition of a continuous-time Markov process. To model the bed load transport with a continuous-time Markov process, here we define two additional motion states, i.e., states 3 and 4, to restructure the random process given in Figure 1. State 3 is to replace

the state 1 that follows a state 1, while state 4 is to replace the state 2 that follows a state 2. Accordingly, the state transitions $1 \rightarrow 1$ and $2 \rightarrow 2$ become $1 \rightarrow 3$ and $2 \rightarrow 4$, respectively (as shown in Figure 1). This is what we call ‘pseudo four-state’ because in fact there are only two motion states, namely, static and moving. With this revision, a direct application of the properties of a continuous-time Markov process is made possible.

[9] The primary merit of using a continuous-time Markov process to model the movement of bed load particles is that the limiting (or long-run) probability of a bed load particle being in the moving state can be readily evaluated with the following equation (derivation see Appendix A):

$$P_{M,i} = \frac{P_{E,i}}{P_{E,i} + R_{T,i}(1 - P_{E,i})} \quad (3)$$

where $P_{M,i}$ = limiting probability that a bed load particle of fraction i is in the moving state, which can be interpreted as the long-run proportion of time that a bed load particle of fraction i is in the moving state; $P_{E,i}$ = instantaneous probability of particle entrainment (for fraction i); $R_{T,i} = T_{S,i}/T_{M,i}$ = ratio of mean holding time (see section 4.5), where $T_{S,i}$ and $T_{M,i}$ = mean single-step holding time in the static and moving states, respectively (for fraction i). The instantaneous entrainment probability $P_{E,i}$ can be evaluated with the method recently presented by *Wu and Chou [2003a]*, which is a most updated version of entrainment probability that incorporates the randomness of turbulent fluctuation and bed grain geometry, meanwhile takes into account the rolling and lifting modes of incipient motion, thus offers a more comprehensive estimate of the entrainment probability. Their results are demonstrated in Figure 2, where it is shown that the entrainment probabilities vary as a function of the dimensionless effective shear stress θ'_i (the definition of θ'_i is given in section 4.2). Rolling and lifting, identified by whether the entrained particle is lifted off the bed, are two independent modes of entrainment [*Wu and Chou, 2003a*]. The lifting probability $P_{L,i}$ increases monotonously with θ'_i , whereas the rolling probability $P_{R,i}$ increases with θ'_i in the region of $\theta'_i < 0.15$ but then reduces for larger values of θ'_i . The total entrainment probability $P_{E,i}$ (= the sum of rolling and lifting probabilities) is well approximated by the cumulative lognormal distribution of θ'_i , with a mean of 0.240 and standard deviation of 0.268 ($R^2 = 0.99$), i.e., $\text{LN}(0.240, 0.268)$ can be practically incorporated into (3) for evaluating $P_{M,i}$. It should be noted here that the limiting probability $P_{M,i}$ is a long-run probability of the

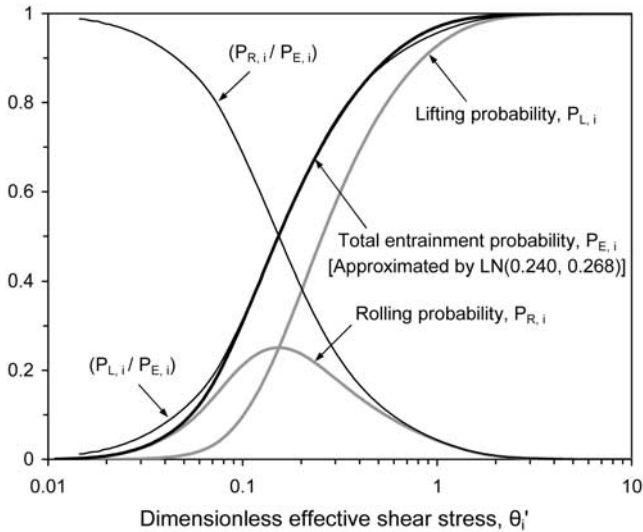


Figure 2. Variations of rolling probability $P_{R,i}$, lifting probability $P_{L,i}$, total entrainment probability $P_{E,i}$, $P_{R,i}/P_{E,i}$, and $P_{L,i}/P_{E,i}$ with dimensionless effective shear stress. The $P_{E,i}$ and $P_{L,i}/P_{E,i}$ curves can be well approximated by cumulative lognormal distributions LN(0.240, 0.268) and LN(0.259, 0.328), respectively.

random process being in the moving state, whereas $P_{E,i}$ is an instantaneous probability of particle entrainment at the single-step points. It should be also mentioned that the single-step holding time in state m , defined as the amount of time a bed load particle spends in state m for a single-step motion, is a memoryless random variable and must thus be exponentially distributed [see, e.g., Ross, 2000; Nelson, 1995], which is an underlying assumption that needs to be justified experimentally (see section 4.5).

3.2. Formulation of Fractional Transport Rate

[10] Here we present the formulation of fractional transport rate for the partially mobilized mixed-size sediment. To avoid repeating, it is claimed that the formulation presented herein is for grains of fraction i , denoted by a subscript. The number of grains of fraction i per unit bed area can be approximated by f_i/D_i^2 , where D_i = grain diameter of fraction i [Wilcock, 1997]. Multiplying f_i/D_i^2 by Y_i gives the number of active grains per unit area, denoted as N_i . If the movement of these active grains follows a continuous-time Markov process, during a sufficiently long transport event, the number of grains staying in the moving state at any moment can be evaluated by $N_i P_{M,i}$, per unit area. These moving particles averagely advance a distance of L_i in a time period $T_{M,i}$, where L_i = mean single step length, $T_{M,i}$ = mean single-step holding time in the moving state. As such, the number of grains that can be collected at a sampling section in a time period $T_{M,i}$ is $N_i P_{M,i} L_i$ per unit width (illustrated in Figure 3), which is multiplied by the mass of a grain, m_i , and divided by $T_{M,i}$ to yield the unit width mass transport rate, i.e.,

$$q_{bi} = \frac{N_i P_{M,i} L_i m_i}{T_{M,i}} = \left(\frac{\pi}{6} \rho_s\right) \left[D_i f_i Y_i P_{M,i} \left(\frac{L_i}{T_{M,i}} \right) \right] \quad (4)$$

where $m_i = \pi D_i^3 \rho_s / 6$, ρ_s = density of sediment. All terms in the brackets of (4) are relevant to fraction i , which include

grain diameter, proportion on the bed, fractional mobility, long-run probability in the moving state, and $L_i/T_{M,i}$. This last term is taken to be the mean particle velocity, which is nondimensionalized as $V_{p,i} = (L_i/T_{M,i}) / \sqrt{(\rho_s/\rho - 1)gD_i}$, where $V_{p,i}$ is dimensionless mean particle velocity and shown to vary with the dimensionless effective shear stress θ'_i (see section 4.4), ρ = density of water, g = gravitational acceleration. It is noted that the form of (4) is slightly similar to the previous result obtained by Sun and Donahue [2000] in that they are both proportional to $D_i, f_i, P_{M,i}$, and $V_{p,i}$. However, in their equation, a $P_{M,i}/P_{S,i}$ rather than a $P_{M,i}$ was present, primarily due to that they used binomial distributions to evaluate the mean numbers of particles in the static and moving states, which would undesirably make their predicted value of q_{bi} approach to infinity as θ'_i becomes large and $P_{E,i} \rightarrow 1$. The transport rate predictor given by equation (4) is formulated with the surface-based parameters. In practical applications, however, a correction for the subsurface entrainment of fully mobilized fractions should be incorporated. In addition, the effect of sporadic movement of partially mobilized fractions must be taken into account. These corrections are described below.

3.3. Corrected Fractional Transport Rate

[11] The corrected form of the unit width fractional transport rate is given by

$$q_{bi} = \left[\left(\frac{\pi}{6} \rho_s\right) \left(D_i f_i Y_i P_{M,i} V_{p,i} \sqrt{(\rho_s/\rho - 1)gD_i} \right) \Delta_i Y_i^{1.8} \right] \quad (5)$$

All the terms in the brackets of (5) are equivalent to those terms in (4), but here we incorporate a subsurface entrainment factor Δ_i and a partial mobility factor $Y_i^{1.8}$ to correct for the fully and partially mobilized fractions, respectively.

3.3.1. Correction for Fully Mobilized Fractions

[12] Under the partial transport condition, some finer-grained fractions can be fully mobilized while the others are partially mobilized. For those fully mobilized fractions, it is insufficient to count only the surface grains as the source of bed load because the grains in the subsurface layer could be also entrained. The form of equation (4) is likely to underestimate the transport rates of the fully mobilized fractions, thus a subsurface entrainment correction factor Δ_i needs to be introduced. Such a correction factor is related to the exchange depth [Wilcock, 1997], which varies as a complicated function of bed shear stress and grain size. Nevertheless, a simplified Δ_i can be obtained from the limiting condition of full transport. Laboratory and field

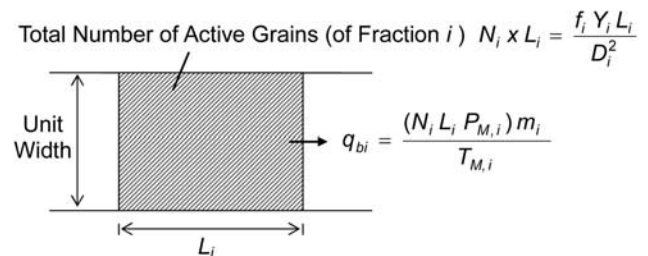


Figure 3. Definition sketch showing the formulation of unit width fractional transport rate.

observations have indicated that the depth of sediment exchange associated with full mobilization of bed surface approaches twice the thickness of surface layer [Wilcock and McArdell, 1997; Haschenburger and Wilcock, 2003], implying that two layers (surface and subsurface layers) of fully mobilized fractions could be entrained. For such limiting case, the fractional transport rates predicted by equation (4) should be multiplied by a factor of 2 to account for the effect of two-layer entrainment. It is worth noting that $\Delta_i = 2$ is a simplified correction factor based on an assumption that the surface and subsurface compositions are identical (i.e., vertical sorting is not considered herein), which is used to correct the uniform-type underestimation of the fully mobilized fractional transport rates (see section 5.1). On the other hand, for those finest fully mobilized size fractions, the effective shear stress tends to be underestimated because of the excessively overestimated hiding effect, leading to a nonuniform-type underestimation of the fractional transport rates, the correction factors for these finest fractions are grain-size dependent. A set of Δ_i for these two types of underestimation is given by

$$\Delta_i = \begin{cases} 2 & \text{for uniform-type underestimation} \\ (q_{bj}/f_j)/(q_{bi}/f_i) & \text{for nonuniform-type underestimation} \end{cases} \quad (6)$$

where q_{bj}/f_j = fractional transport rate predicted with (4) for a fraction j whose $Y_j = 0.99$; q_{bi}/f_i = fractional transport rate predicted with (4) for a fraction i whose $Y_i = 1$. This correction for the nonuniform-type underestimations results in an identical value of q_{bi}/f_i ($= q_{bj}/f_j$) for all the fully mobilized fractions and thus ensures equal mobility (i.e., $Y_i = 1$) of those fractions. Note that the corrections for the nonuniform-type underestimation are required only if the predicted transport rates of the finest size fractions obviously deviate from those of other fully mobilized fractions (see section 5.1). It should be also mentioned that the previous full transport model of Sun and Donahue [2000] achieved a reasonably good agreement with the experimental data without introducing the subsurface entrainment factor, which is not meant to indicate that such a correction is unnecessary. Rather, their fit to the observed data was assured through direct and indirect calibrations of many of the empirical parameters in their model.

3.3.2. Correction for Partially Mobilized Fractions

[13] As we compared the observed fractional transport rates with the predicted results of (4), we found that equation (4) consistently overestimates the transport rates of the partially mobilized fractions, implying that the sporadic grain movement of the partially mobilized fractions must have had a greater effect on the fractional transport rate than expected. To correct this, a possible alternative is to multiply equation (4) by a partial mobility factor. On the basis of an analysis of the laboratory and field data for which the fractional mobility is known (including the data from our own flume studies, BOMC experiments [Wilcock and McArdell, 1997], and Goodwin Creek [Kuhnle, 1992]), we obtain a correction factor $Y_i^{1.8}$ that gives the best fit results to the observations. This correction factor is particularly important for the coarse grains with low fractional mobility. For exam-

ple, for a typical size fraction with $Y_i = 0.3$, the corrected transport rate is approximately one order lower than the value given by equation (4). In this regard, the partial mobility factor, as compared to Δ_i , seems to have more weight on the model results. As revealed by equation (5), the correction factor $Y_i^{1.8}$ makes the fractional transport rate proportional to $Y_i^{2.8}$ overall, which is similar to an independent result of Sun and Donahue [2000] gained by analyzing the partial transport data from East Fork River [Leopold and Emmett, 1977]. Note that the correction factor $Y_i^{1.8}$ is effective exclusively for the partially mobilized fractions since $Y_i = 1$ exerts no effect upon equation (5).

4. Determination of Model Parameters

[14] The stochastic partial transport model presented in equation (5) contains several parameters to be determined experimentally, which include two physical parameters, Y_i and $V_{p,i}$, and a stochastic parameter, $P_{M,i}$ (or equivalently $R_{T,i}$). These parameters vary as a function of the dimensionless effective shear stress. Details of the experimental study, effective shear stress, and model parameters are described in the subsequent sections.

4.1. Experimental Study

[15] The experimental study was conducted in a 40-cm-wide 12-m-long tilting flume located at the Hydrotech Research Institute, NTU. A tailgate at the downstream end was used to maintain a quasi-uniform flow in the 3.6-m gravel-sand bed working section at the middle of the flume, downstream of this section was a bed load trap installed in the bottom of the flume. The slope of the flume was adjusted to 1/300. A Hitachi KP-F100C 10-bit digital CCD camera was used to photograph the bed surface or to record the movement of bed load particles in the 1.2-m observation section (middle of the working section), as shown in Figure 4. The 1300×1030 pixels resolution of the CCD camera enabled us to create pictures suitable for the image analysis. The recording device, interfaced by PIXCI D2X imaging board, was connected to a data logging system with a RAID (Redundant Array of Independent Drives) serving to store an extremely huge amount of motion-picture images taken during a transport event. A floating acrylic plate (sufficiently light such that the flow was not much interfered) was placed on the wavy surface of water to lesson the image distortion [see Drake et al., 1988].

[16] Two types of experiments, one with the colored bed and the other with the plain bed (both in plane configuration), were carried out to investigate the fractional mobility and movement of bed load particles, respectively. For the former, the experiments were similar to those performed by Wilcock and McArdell [1993, 1997]. The sediment was separated into six size fractions, each painted with a different color. The proportion, grain size, and color of each fraction are listed in Table 1. The sizes of the grains covered a range between 1.4 and 12.7 mm, with a median size $D_{50} = 4$ mm. The mean specific gravity of the sediment was 2.65. The collected bed load sediment was periodically returned to the flume from the upstream end of the working section (the time interval of this action, ranging from 20 minutes to 3 hours,

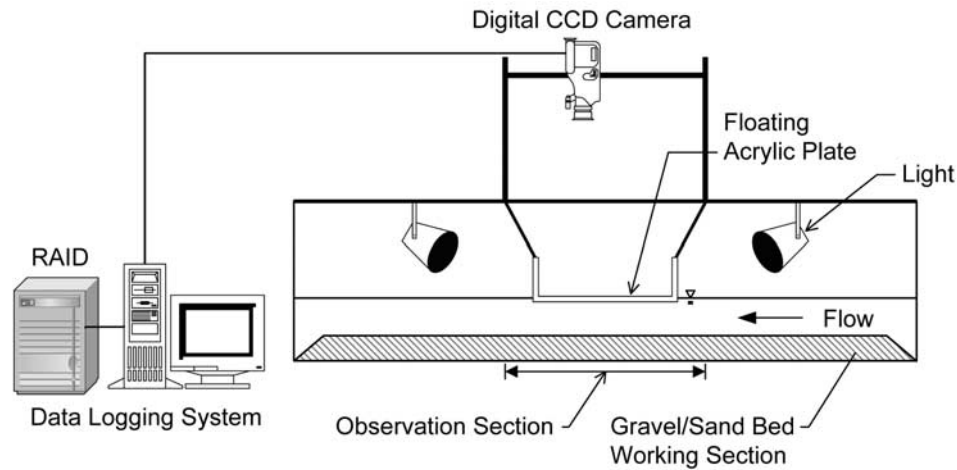


Figure 4. Schematic diagram of experimental setup. The 1.2-m observation section is in the middle of the 3.6-m gravel-sand bed working section.

was dependent upon the bed load transport rate). The partial transport experiments were lasted for sufficient time (see Table 2) to reach equilibrium bed load transport (confirmed by the bed load samples) and quasi-steady mobility (confirmed with the time criteria proposed by *Wilcock and McArdell* [1997]). The last bed load sample collected before the end of a run was used to evaluate the equilibrium transport rate. For each run, the initial and final states of the bed surface were photographed. Each picture was adjusted to cover an area of $20 \times 30 \text{ cm}^2$ (width by length) due to the desirable resolution. Four pictures were taken to cover the 1.2-m-long observation section. The initial and final images were then analyzed using the XCAP image analysis software (EPIX Inc.), yielding a set of data concerning the fractional mobility (for details, see section 4.3). A total of 7 runs were performed with various flow conditions, which together with the total bed load transport rates, are provided in Table 2. These flows were all associated with the partial transport condition, no full bed load transport was observed.

[17] For the second type of experiments, a number of grains with different colors were supplied onto the plain gravel-sand bed from the upstream working section. For each run, the movement of the colored grains was recorded with the fixed CCD camera for 3 hours (due to the capacity limit of RAID). A total of 5 runs were performed with different flows, including four corresponding to the partial transport and one at the margin of full transport (see Table 3). The digital images were analyzed with the aid of the XCAP software for evaluating the mean particle velocity (for details, see section 4.4). The motion pictures were also reviewed manually for identifying the single-step points of the particle

movement, which were then used to estimate the ratio of mean holding time in the static and moving states (for details, see section 4.5).

4.2. Effective Shear Stress

[18] To account for the hiding-exposure effect of the mixed-size sediment, an appropriate form of hiding factor is required. Two types of hiding factor are generally available, one is to correct the critical (or reference) shear stress for incipient motion, while the other is to correct the shear stress applied on the sediment particle. Most of the reported hiding factors belonged to the first category [e.g., *Bridge and Bennett*, 1992; *Wu et al.*, 2000; *Shvidchenko et al.*, 2001; *Wilcock and Crowe*, 2003], only several considered the relative size effect on the applied shear stress [e.g., *Proffitt and Sutherland*, 1983; *Misri et al.*, 1984; *Sun and Donahue*, 2000]. It is generally accepted that the critical shear stress for the particle coarser than median (or mean) size should be lower than the threshold value corresponding to the equivalent uniform size because the coarser particle is more exposed to the flow, but the critical shear stress for the finer particle should be higher because it is more likely sheltered by the coarse particles. However, this problem can be tackled with a different approach. That is, the effective shear stress applied on the coarser particle should be higher than the shear stress evaluated from the mean roughness, whereas the effective shear stress applied on the finer particle should be smaller than the mean bed shear stress.

Table 1. Proportion, Grain Size, and Color of Each Fraction of Bulk Sediment

Fraction i	Color	Grain Size D_i , mm	Proportion, %
1	yellow	1.68	14
2	green	2.59	22
3	black	3.67	15
4	purple	5.04	16
5	blue	7.78	20
6	red	11.0	13

Table 2. Flow Conditions and Bedload Transport Rates of Colored Bed Experiments

Run	Flow Depth h , cm	Mean Velocity U , m/s	Bed Shear Stress τ_0 , Pa	Bedload Transport Rate, g/m/s	Duration, hours
C-1	8.0	0.52	2.04	N.A.	72
C-2	9.0	0.55	2.16	0.01	72
C-3	8.5	0.71	3.76	0.64	24
C-4	8.3	0.64	3.08	0.05	48
C-5	8.5	0.78	4.46	1.52	12
C-6	9.2	0.81	4.75	2.80	12
C-7	8.0	0.73	4.06	1.39	24

Table 3. Flow Conditions of Plain Bed Experiments

Run	Flow Depth h , cm	Mean Velocity U , m/s	Bed Shear Stress τ_0 , Pa
P-1	8.5	0.69	2.94
P-2	11.0	0.79	3.49
P-3	9.0	0.96	5.62
P-4	5.8	0.71	3.70
P-5	8.0	0.65	2.71

An entrainment probability that varies as a function of effective shear stress is included in the stochastic bed load model. As such, the effective shear stress described below is used to account for the relative size effect of the mixed-size sediment.

[19] On the basis of a sensitivity analysis, we found that the analyzed data are most sensitive to the following form of dimensionless effective shear stress [Sun and Donahue, 2000]:

$$\theta'_i = \xi_i \theta_i = \left[\sigma_g^{0.25} \left(\frac{D_i}{D_m} \right)^{0.5} \right] \theta_i \quad (7)$$

where ξ_i = hiding factor of fraction i incorporating the geometric standard deviation of the grain size distribution, σ_g , and relative size effect, D_i/D_m , where D_m = mean grain size; $\sigma_g = D_{84}/D_{50}$ for $D_i > D_{50}$, but = D_{50}/D_{16} for $D_i < D_{50}$; $\theta_i = \tau_0/(\gamma_s - \gamma)D_i$ = dimensionless shear stress based on D_i , where τ_0 = mean bed shear stress, γ_s and γ = specific weights of sediment and water, respectively. The bed shear stress τ_0 was evaluated with the flow depth and velocity using the depth-averaged logarithmic profile [Wilcock, 1996]:

$$\frac{U}{u_*} = \frac{1}{\kappa} \ln \left(\frac{h}{ez_0} \right) \quad (8)$$

where U = mean velocity; u_* = bed shear velocity = $\sqrt{\tau_0/\rho}$; κ = von Karman constant, taken to be 0.4 for clear water; h =

flow depth; e = base of the natural logarithms (= 2.718); z_0 = bed roughness length = $D_{65}/30$ [Wilcock and McArdell, 1993].

4.3. Fractional Mobility

[20] The fractional mobility was evaluated by overlapping the initial and final images of the bed surface and identifying the grains that remained immobile. This was done with the aid of blob analysis featured by the XCAP software, which can segment the blobs from the background by the specified target color. The number of blobs can be evaluated by setting the limits on blob width and height for each size fraction. To inspect the accuracy of blob counting, the number of surface grains in each size fraction was evaluated manually with the point counting technique [Wilcock and McArdell, 1993] and used as a basis for comparison. The results indicated that the accuracy for the three coarser fractions (fractions 4 to 6) ranged from 80% to 96%, with a mean of 87%, while the accuracy for the three finer fractions (fractions 1 to 3) ranged from 60% to 86%, with a mean of 74%. The accuracy of blob counting for the coarser grains was acceptable. However, for the finer fractions, the point counting method was used. Because the analysis of fractional mobility needs to identify the immobile grains on the final images, which involves some judgments that are not supported by the software, this task was done manually. Figure 5 is a demonstration of the initial and final images of the bed surface. Shown in Figure 5a is the initial number of blue grains in each grid, while illustrated in Figure 5b is the number of blue grains identified as immobile in each grid. Each image was divided into 4×4 grids for the three coarser fractions, while the image was divided into 8×8 grids for the three finer fractions. The total number of immobile grains divided by the initial number of grains in that fraction yields the proportion of immobile grains. The fractional mobility was then evaluated by subtracting the immobile proportion from unity.

[21] The results of fractional mobility so obtained are given in Table 4. The mobility generally increased with the

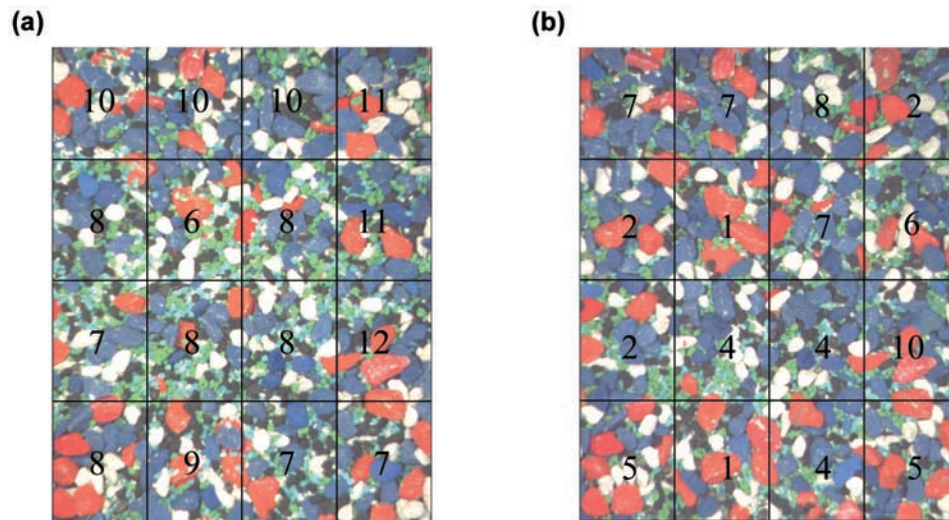


Figure 5. Photographs demonstrating (a) initial and (b) final images of bed surface. Figure 5a shows the initial number of blue grains in each grid, while Figure 5b shows the number of blue grains identified as immobile in each grid. Each picture covers an area of 20×30 cm² (width by length).

Table 4. Fractional Mobility and Surface Proportions of Colored Bed Experiments

Run	Fractional Mobility						Surface Proportions					
	Y_1	Y_2	Y_3	Y_4	Y_5	Y_6	f_1	f_2	f_3	f_4	f_5	f_6
C-1	0.92	0.78	0.47	0.12	0.03	0	0.029	0.09	0.105	0.089	0.349	0.337
C-2	0.98	0.86	0.74	0.56	0.34	0.15	0.013	0.066	0.118	0.107	0.393	0.303
C-3	1.0	0.98	0.83	0.72	0.54	0.25	0.009	0.061	0.058	0.096	0.406	0.371
C-4	1.0	0.92	0.78	0.62	0.47	0.21	0.008	0.087	0.082	0.088	0.395	0.339
C-5	1.0	1.0	1.0	0.95	0.93	0.75	0.008	0.077	0.072	0.086	0.392	0.365
C-6	1.0	1.0	1.0	0.98	0.95	0.84	0.008	0.094	0.057	0.076	0.362	0.402
C-7	1.0	1.0	0.95	0.92	0.78	0.44	0.017	0.134	0.110	0.097	0.343	0.298

bed shear stress but decreased with the grain size, which is consistent with the results presented in a previous work [Wilcock and McArdell, 1997]. For example, the mobility of the coarsest fraction was as low as zero in run C-1 (which corresponded to the smallest τ_0 of all); however, five fractions exceeded 95% mobility in run C-6 (which corresponded to the largest τ_0 of all), with the finer three fractions in full mobility. To quantify this trend, the fractional mobility Y_i was plotted against θ'_i as illustrated in Figure 6, where it is shown that the variation trend between Y_i and θ'_i may well be approximated by a cumulative lognormal distribution LN(0.0287, 0.0082), with $R^2 = 0.89$. The fractional mobility Y_i becomes vanishingly small for $\theta'_i < 0.01$, whereas full mobility can be reached for $\theta'_i > 0.06$. The fractional mobility observed in our experiments is relatively smaller than the previous results [Wilcock and McArdell, 1997], with the value $Y_i = 0.9$ occurring at $\theta'_i \approx 0.04$ in the present experiments but at a smaller value of $\theta'_i \approx 0.034$ in the previous study, which is attributed to the smaller proportion of sand in our gravel-sand mixture. The effect of sand content on the fractional mobility of mixed-size sediment is further investigated in section 6.

4.4. Mean Particle Velocity

[22] The movement of individual colored grains was recorded with the sequence capture at a speed of 4 images per second and stored as a video file in the RAID, which was converted to an image file and reviewed manually in search of the usable events. For

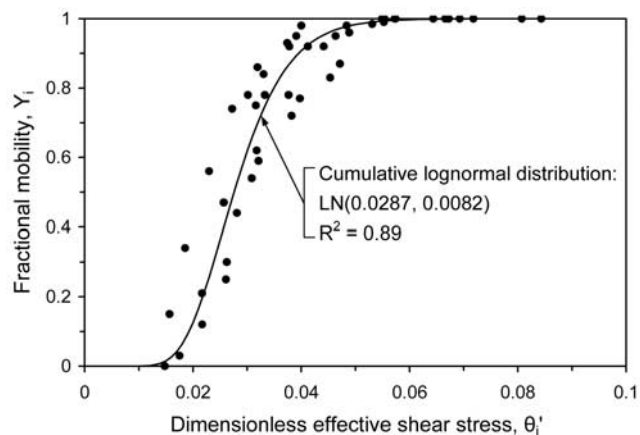


Figure 6. Relation between fractional mobility and dimensionless effective shear stress (data from run C-1 ~ C-7). The variation trend can be represented by a cumulative lognormal distribution LN(0.0287, 0.0082).

example, demonstrated in Figure 7 is an event of particle movement usable for the analysis. The picture shows that at a moment a blue-colored grain entered the observation area from the upstream (right side); after a series of continuous movements the target grain moved out of the area. With the function of particle tracking of the XCAP software, the grain trajectory was traced. Given the coordinates of each track point and the time interval between two consecutive points ($=0.25$ s), five velocity data can be obtained from this event. Through such procedures, we have acquired the mean velocities of various size fractions under five different flows (Table 3) corresponding to a range of θ'_i between 0.03 and 0.1. These velocities were nondimensionalized by $\sqrt{(\rho_s/\rho - 1)gD_i}$, which are shown in Figure 8 with a best fit function of θ'_i ($R^2 = 0.92$) given by

$$V_{R,i} = 0.305 \ln(\theta'_i) + 1.4 \quad (9)$$

where $V_{R,i}$ = dimensionless mean velocity for fraction i . By extrapolating (9), it is found that $V_{R,i} = 0$ at $\theta'_i \approx 0.01$, which is consistent with the results shown in Figure 6 (fractional mobility) and Figure 2 (entrainment probabilities) in that surface grains become immobile for $\theta'_i < 0.01$. During our experiments, we have observed that nearly all the particle movements occurred in the rolling

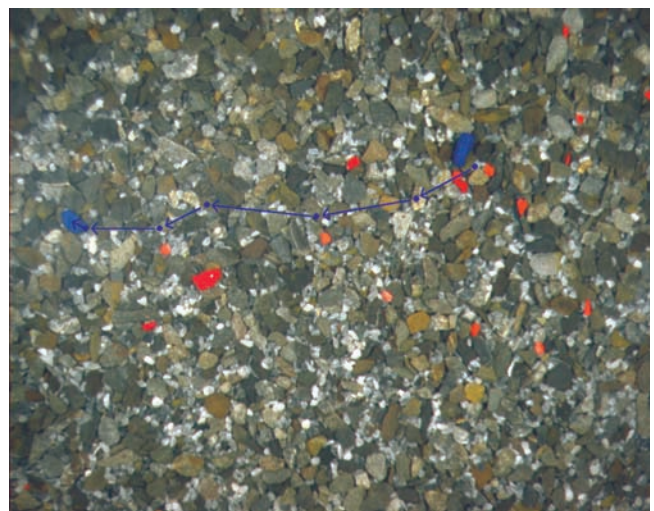


Figure 7. Photograph demonstrating the continuous trajectory of a blue-colored grain. The time interval between two consecutive points is 0.25 s. The picture covers an area of 35×45 cm². Flow is from right to left.

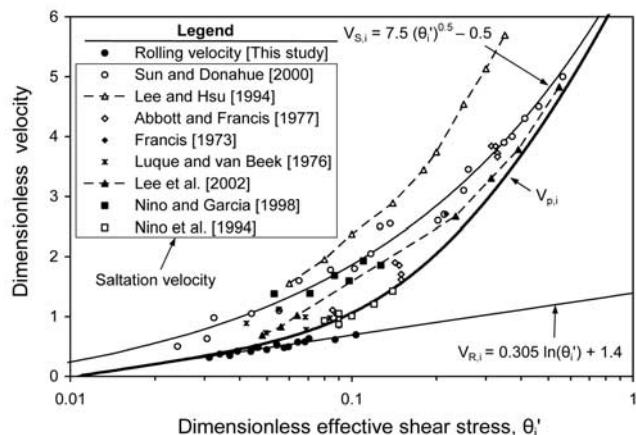


Figure 8. Rolling, saltation, and mean particle velocities versus dimensionless effective shear stress. The saltation velocities of *Niño et al.* [1994] lie perfectly on the $V_{p,i}$ curve.

mode, only very rarely in saltation. These observations can be further confirmed with the entrainment probabilities shown in Figure 2. For our test range of θ'_i between 0.03 and 0.1, the rolling probability is much greater than the lifting probability; even for $\theta'_i = 0.1$, the rolling probability is greater than twice of the lifting probability. As such, the result presented in (9) may well be used to represent the mean rolling velocities. Moreover, the mean particle velocity is assumed here as a weighted average value of all possible modes, including the sliding, rolling, and saltation. Among which, the sliding mode is less important and often neglected in the analysis [*Wu and Chou*, 2003a]. Thus, to seek the mean particle velocity, we need an appropriate estimate of the saltation velocity, which is described below.

[23] Many researchers have devoted to the study of saltation velocities [e.g., *Bridge and Dominic*, 1984; *Gordon et al.*, 1972; *Wiberg and Smith*, 1985; *Sekine and Kikkawa*, 1992; *Niño et al.*, 1994; *Niño and García*, 1998; *Lee et al.*, 2002]. Previous efforts were mostly focused on the single-particle saltation velocities [e.g., *Francis*, 1973; *Abbott and Francis*, 1977; *Lee and Hsu*, 1994; *Sun and Donahue*, 2000]; only recently was the continuous saltation process of multiple particles systematically studied [e.g., *Lee et al.*, 2002], and Figure 8 demonstrates a compilation of these data. It is shown that the saltation velocities of *Lee and Hsu* [1994] are the highest because their data were measured from the experiments with the single-step saltation of a single particle, hence no energy was lost through the collisions with the bed surface and other particles. However, the saltation velocities of *Lee et al.* [2002] are much smaller because they were acquired from the continuous saltating process of multiple particles, thus considerable energy was lost through the particle-bed and interparticle collisions. The saltation data of *Sun and Donahue* [2000] and *Niño and García* [1998] are consistent and lie between the upper and lower data sets of *Lee and Hsu* [1994] and *Lee et al.* [2002]. The data of *Francis* [1973] and *Abbott and Francis* [1977] were measured from the experiments of single grains moving over a fixed bed, while the data of

Luque and van Beek [1976] were obtained from the low transport rates over a loose bed. The saltation velocities gained by *Sun and Donahue* [2000] are among the most comprehensive data, covering a widest range of θ'_i between 0.02 and 0.6. On the basis of their data, *Sun and Donahue* [2000] presented an empirical relation for the mean saltation velocity:

$$V_{S,i} = 7.5(\theta'_i)^{0.5} - 0.5 \quad (10)$$

where $V_{S,i}$ = dimensionless saltation velocity for fraction i . Figure 8 shows that the rolling velocities are consistently smaller than the corresponding saltation velocities. With the pure rolling and saltation velocities given by equations (9) and (10), respectively, we can now proceed to evaluate the mean particle velocity by incorporating the entrainment probabilities.

[24] Given the probabilities of entrainment in the rolling and lifting modes (Figure 2), we propose that the mean velocity of a bed load particle (for fraction i), denoted as $V_{p,i}$, is determined by the weighted average of the rolling and saltation velocities, as expressed by

$$V_{p,i} = \left(\frac{P_{L,i}}{P_{E,i}}\right)V_{S,i} + \left(\frac{P_{R,i}}{P_{E,i}}\right)V_{R,i} \quad (11)$$

where $P_{L,i}/P_{E,i}$ = proportion of lifting probability in the total entrainment probability (see Figure 2), approximated by a cumulative lognormal distribution of θ'_i , i.e., $\text{LN}(0.259, 0.328)$, with $R^2 = 0.99$; and $P_{R,i}/P_{E,i}$ is simply evaluated by $1 - P_{L,i}/P_{E,i}$. The mean particle velocity so obtained is illustrated in Figure 8, where the $V_{p,i}$ curve asymptotically approaches $V_{R,i}$ and $V_{S,i}$ at very small and large values of θ'_i , respectively. Although there are no data available for the rolling velocity at larger values of θ'_i and thus the extrapolation of equation (9) beyond the limit of measurements is subjected to uncertainty, it is found that the rolling probabilities associated with those large values of θ'_i are so small that the extrapolated $V_{R,i}$ does not make significant differences to the results of $V_{p,i}$. As demonstrated in Figure 8, the $V_{p,i}$ curve appears to be the frontier of the observed saltation velocities, confirming that saltation velocities are greater than the corresponding mean particle velocities. It is speculated that the gravel saltation data of *Niño et al.* [1994] are the mean particle velocities (i.e., including saltation and rolling velocities) and thus lie perfectly on the $V_{p,i}$ curve.

4.5. Ratio of Mean Holding Time

[25] To evaluate the ratio of mean holding time in static and moving states, the single-step points of the movement of colored grains were identified manually by reviewing the motion pictures. This procedure was repeated by two individuals, aiming to obtain a minimum biased result. The data of single-step holding time were then ranked and used to plot the diagrams of exceeding probability; Figure 9 illustrates some typical examples of such graphs for the static and moving states. As discussed in section 3.1, for a continuous-time Markov process the single-step holding time in state m is an exponentially distributed random variable. Given the mean value of the

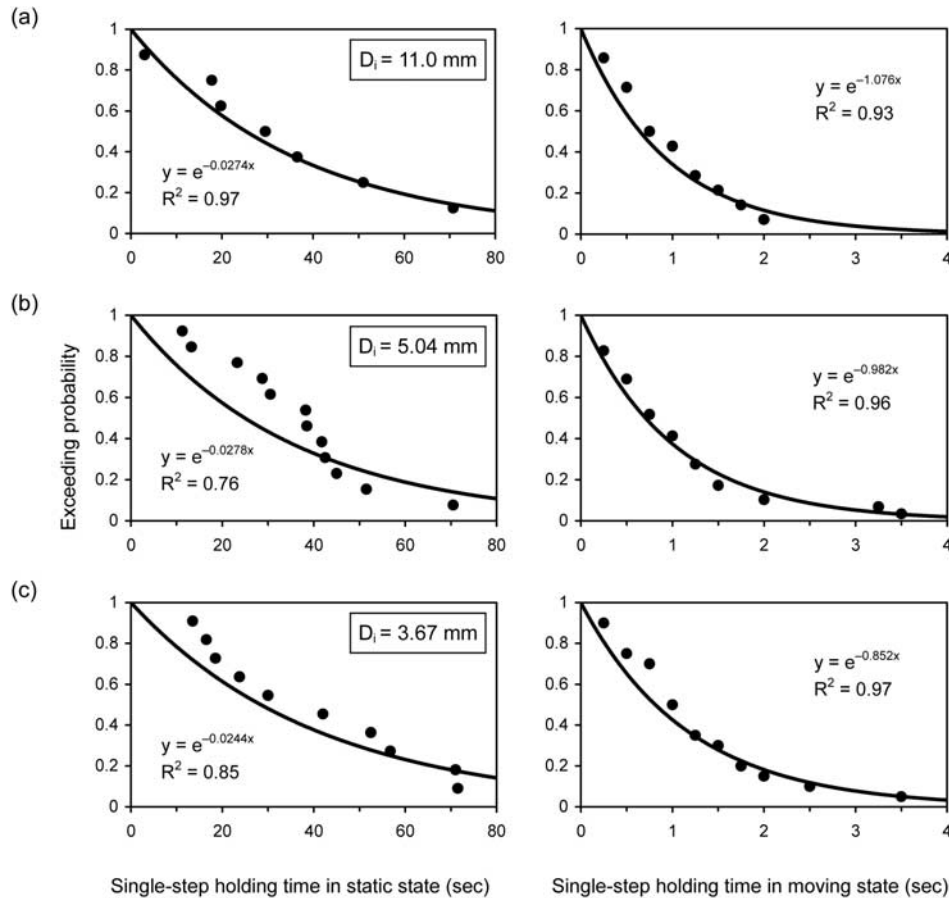


Figure 9. Diagrams of exceeding probability versus single-step holding time in static and moving states for different size fractions, D_i = (a) 11.0 mm, (b) 5.04 mm, and (c) 3.67 mm (data from run P-1). The exceeding probabilities are well fitted by the exponential distribution $\exp(-v_{m,i}t)$, $v_{m,i}$ = mean transition rate in state m (for fraction i) = $1/T_{m,i}$, $T_{m,i}$ = mean single-step holding time in state m .

exponential distribution = $1/v_{m,i}$, the exceeding probability for the single-step holding time t can be expressed as $\exp(-v_{m,i}t)$ [see, e.g., Ross, 2000], where $v_{m,i}$ = mean transition rate in state m (for fraction i). It is revealed in Figure 9 that the exceeding probabilities of the single-step holding time are well fitted by the above exponential form, especially for the moving state (with all values of $R^2 > 0.9$), confirming the hypothesis that bed load movement can be modeled as a continuous-time Markov process. The single-step holding time is generally much shorter in the moving state than in the static state, which agrees with the observations made by Einstein [1937]. It is also shown that the single-step holding time in the moving state is consistently less than 4 s, with more than 80% of the data < 2 s; while the maximum single-step holding time in the static state can exceed 1 minute, with more than half of the data > 30 s.

[26] The mean holding time in static state $T_{S,i}(=1/v_{S,i})$ and moving state $T_{M,i}(=1/v_{M,i})$ can be determined from those best fit mean transition rates $v_{S,i}$ and $v_{M,i}$ as illustrated in Figure 9. Variations of some mean resting and moving time with θ'_i are shown in Figures 10a and 10b, from which two findings can be acquired. First, under the same bed shear stress, the mean resting time is longer for the smaller grains but shorter for the larger

ones (Figure 10a), which are mainly due to the more hidden (or sheltered) configuration of the smaller grains and more exposed configuration of the larger ones. However, once entrained, the smaller grains can move for a longer period of time than the larger ones (Figure 10b). In other words, under a given flow the smaller grains are associated with the lower mean transition rates, either from moving to resting or from static to moving. Second, for a size fraction, the mean resting time decreases with the increase of bed shear stress, which is consistent with the results obtained by Niño and García [1998] from the sand saltation experiments (data shown in Figure 10a). Moreover, Figure 10b demonstrates that the mean moving time also declines with the increase of bed shear stress. The shorter mean resting and moving time associated with the greater value of bed shear stress imply that the transitions of motion state occur more frequently at higher flow intensity.

[27] The decline of $T_{S,i}$ with bed shear stress is more substantial than that of $T_{M,i}$. According to our data, the percentage of reduction in $T_{S,i}$ is averagely 8% greater than that in $T_{M,i}$, leading to the results as shown in Figure 10c, where the ratio of mean holding time in static and moving states $R_{T,i}$, defined as $T_{S,i}/T_{M,i}(=v_{M,i}/v_{S,i})$, decreases with the increase of θ'_i . A set of $R_{T,i}$ values

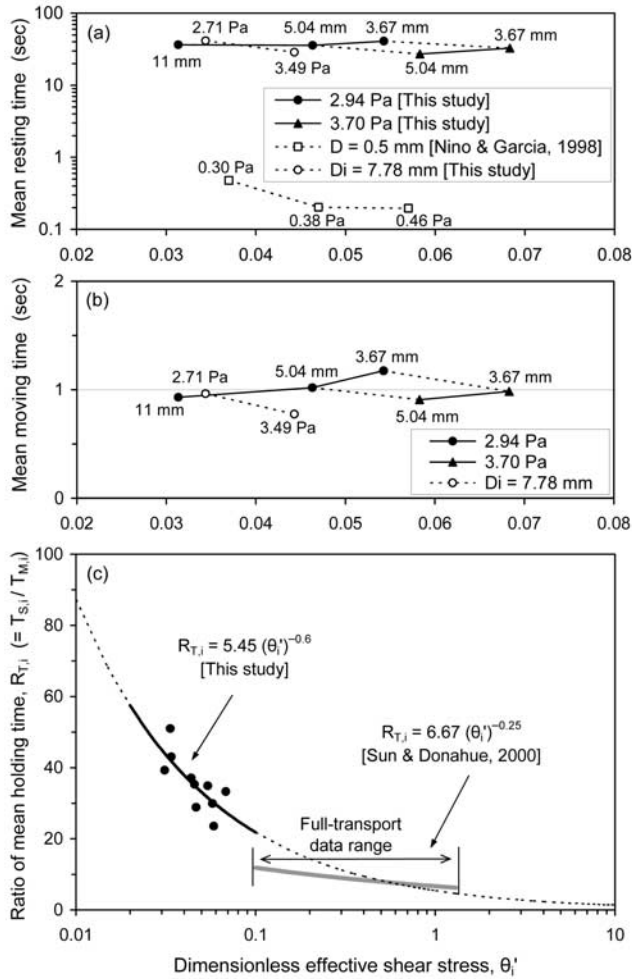


Figure 10. Variations of (a) mean resting time, (b) mean moving time, and (c) ratio of mean holding time with dimensionless effective shear stress (data from run P-1 ~ P-5).

ranging from 20 to 50 was obtained in the present study, and a best fit curve is given by

$$R_{T,i} = 5.45 (\theta'_i)^{-0.6} \quad (12)$$

Note that (12) is not only intended to fit our partial transport data but also extrapolated beyond the experimental range to match with an empirical curve proposed by *Sun and Donahue* [2000] based on their full transport data (as shown in Figure 10c). Their empirical curve was not gained by directly observing the single-step motions but derived through a calibration procedure, with more than 90% of their θ'_i values ranging between 0.1 and 1.3. Our $R_{T,i}$ curve, although based on the partial transport data, agrees reasonably well with their calibrated $R_{T,i}$ curve for the full transport data range. Thus it is believed that equation (12) provides potentially credible estimates of $R_{T,i}$ for both conditions.

5. Model Tests

[28] Three sets of partial transport data, two from flume experiments and one from field study, were used to test the proposed stochastic model. These data were employed because they contain the information regarding fractional

mobility needed for using our model. In addition, three sets of full transport data, two from flume and one from field studies, were used to demonstrate the application of our model to the prediction of fully mobilized transport.

5.1. Partial Transport

[29] The fractional transport rates obtained from our colored bed experiments, along with the predicted results, are plotted in Figure 11a against the grain size, where solid and dashed lines represent the observed and predicted values of q_{bi}/f_i , respectively, f_i = surface proportion of fraction i evaluated with the point counting method (listed in Table 4). The overall variation trend of the predicted values is in good agreement with that of the observed data. For a given flow, the fractional transport rate q_{bi}/f_i decreases with increase of grain size. This decreasing trend becomes steeper as the bed shear stress is reduced, implying that the difference between the fractional mobility of the finer and coarser grains increases with the decline of bed shear stress (also demonstrated in Table 4). As τ_0 is raised, the number of fully mobilized fractions increases, thus the decreasing trend of q_{bi}/f_i curve becomes milder. As shown in Figure 11a, the model consistently overestimates the transport rates of the finer fractions at two smaller values of τ_0 , which appears to indicate the potential limitation of the model in predicting these extremely low transport rates. However, such discrepancies are not of great practical significance because the bed load transport rates associated with the low shear stress are almost negligible.

[30] The proposed model was also tested with a set of data obtained by *Wilcock and McArdeall* [1997]. The bed material used in their BOMC experiments covers a wide range of grain sizes (0.21–64 mm), and the bed shear stress varies from 2.5 to 7.3 Pa. The results are shown in Figure 11b, where the predicted fractional transport rates are in reasonably good agreement with the observed ones. However, the proposed model invariably underestimates the transport rates of the fully mobilized fractions at the lower shear stress, even though the subsurface entrainment corrections for the uniform-type underestimation have been implemented. As mentioned earlier, for most of the case the compositions of surface and subsurface layers are different, which has great effects on the fully mobilized fractions because release of these fine grains from subsurface takes place actively. The subsurface entrainment correction factor $\Delta_i = 2$ is based on the assumption of identical compositions in the surface and subsurface layers, thus would lead to an underestimation of fractional transport rates if the subsurface layer is composed of a greater amount of fine grains. The discrepancies between the observed and predicted results of this kind are believed to primarily originate from this vertical sorting effect. Such discrepancies could be reduced, as the data regarding subsurface composition and exchange depth become available.

[31] To further test the proposed model with the field data, the fractional transport rates obtained from Goodwin Creek [*Kuhnle*, 1992] were employed. This set of data contains the fractional transport rates associated with six different flows, with τ_0 ranging from 2.17 to 15.98 Pa. The bed sediment was separated into eight fractions, with D_i ranging from 0.35 to 45.25 mm. The fractional mobility Y_i was not given in the original report, but the relative mobility

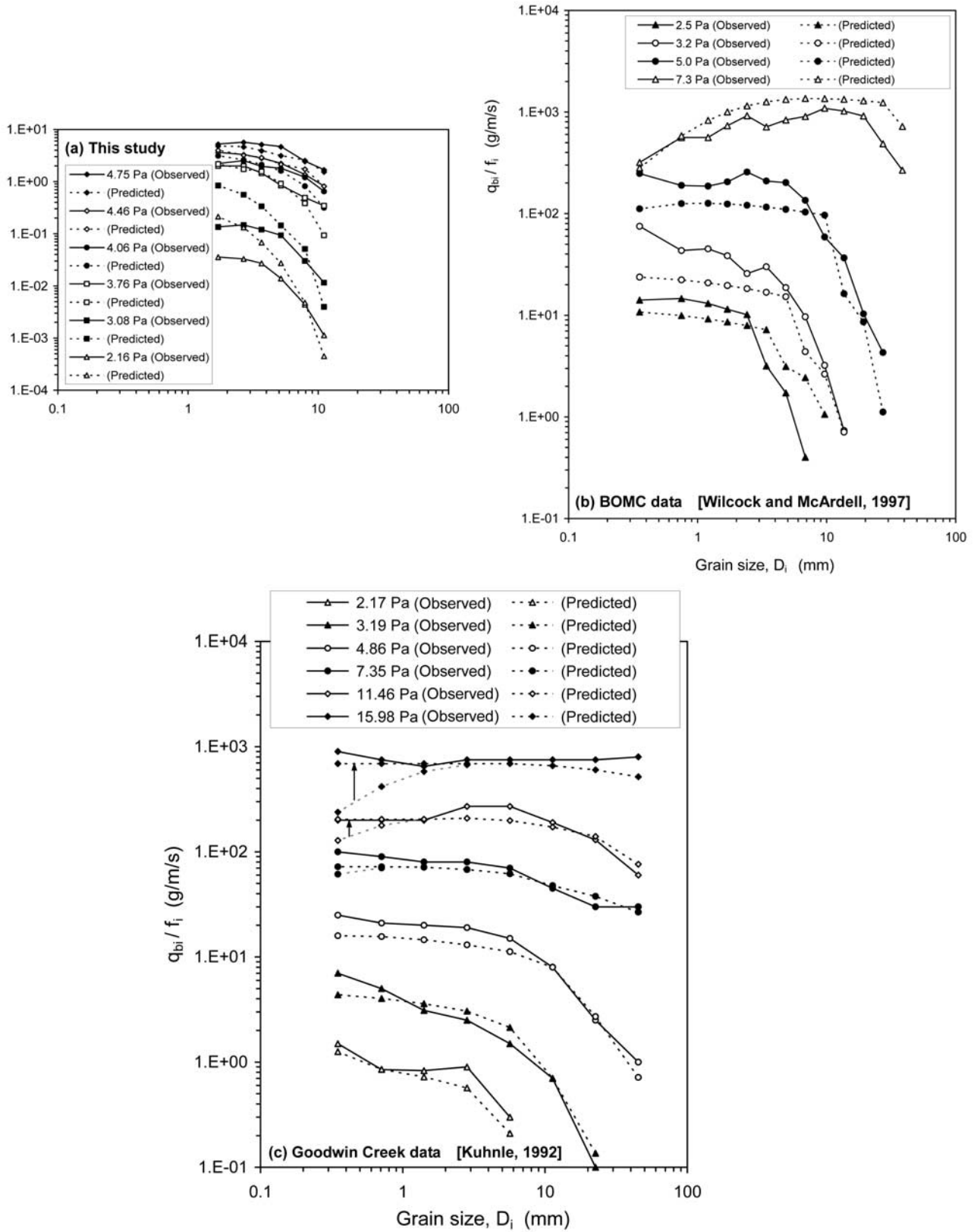


Figure 11. Comparison of predicted and observed fractional transport rates. (a) Run C-2 ~ C-7; (b) BOMC [Wilcock and McArdell, 1997]; (c) Goodwin Creek [Kuhnle, 1992], the predicted results of the original and corrected models are illustrated with the gray and black dashed lines, respectively, evident improvements are demonstrated.

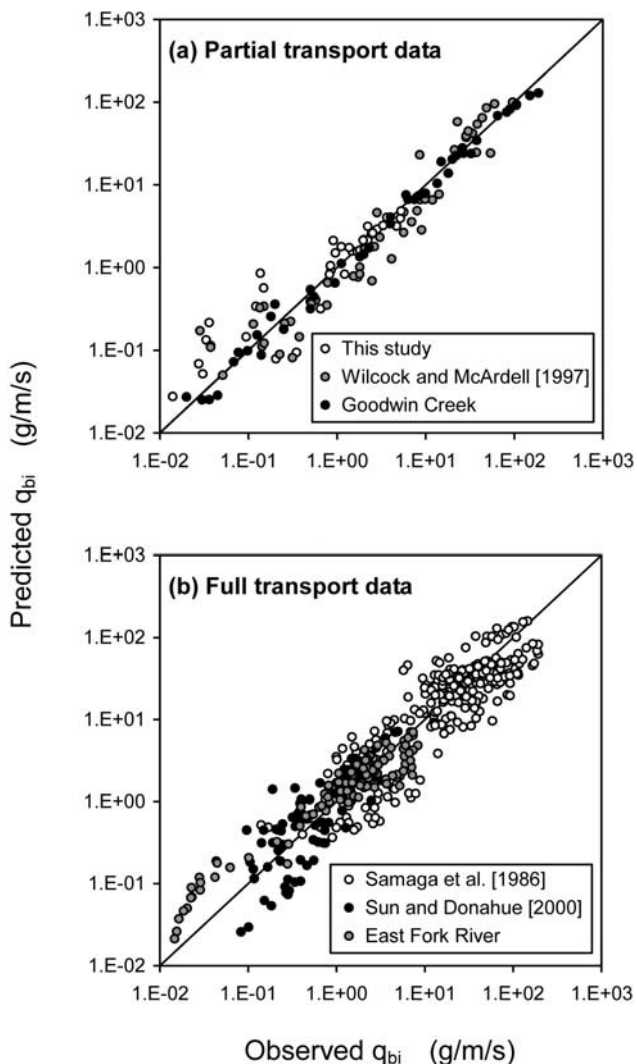


Figure 12. Overall agreement between predicted and observed fractional transport rates for (a) partial and (b) full transport data.

of each fraction p_i/f_i was provided, which was used with (2) to evaluate Y_i . As mentioned earlier, equation (2) is based on a hypothesis that all the active grains can be sampled as bed load and thus only provides a first estimate of Y_i . The correct method to determine Y_i would be using equation (5), as will be discussed in section 6. The predicted and observed fractional transport rates are demonstrated in Figure 11c, where the original predicted results and the corrected ones, given by equations (4) and (5), are illustrated with the gray and black dashed lines, respectively. For three higher values of bed shear stress, it is clearly shown that the original model underestimates the transport rates of the finest size fractions. The improvements are evident after the corrections for the nonuniform-type underestimation (i.e., hiding effect) are implemented. It is noted that a quasi-full transport condition was achieved in Goodwin Creek at the highest flow intensity. For that flow, the q_{bi}/f_i curve appears to be horizontal; the corresponding constant value of q_{bi}/f_i is shown to approach the total bed load transport rate q_b , given that $q_{bi} = q_b p_i$ and $p_i/f_i \rightarrow 1$ under the intensive full transport condition (see section 2). Applications of the

proposed model to the full transport are further tested in the next subsection.

[32] Demonstrated in Figure 12a is an overall comparison of the predicted and observed results of q_{bi} for the three tested data sets. The agreement between the model results and observations is shown generally good. However, as stated earlier, the overestimation of those extremely low transport rates is clearly demonstrated. Additionally, to compare the present model with more common bed load transport formulas, the predicted results of the ubiquitous Meyer-Peter-Müller (MPM) and Einstein-Brown (EB) equations [Julien, 1998] for the BOMC data [Wilcock and McArdell, 1997] are shown in Figure 13. These two equations consistently overestimate the transport rates of the finer fractions but underestimate those of the coarser ones. The overestimation can be as much as of one order of magnitude, while the underestimation can exceed three orders of magnitude. Such results are reasonable because these equations were based on the bed load data of uniform sediment, thus did not take into account the hiding-exposure effect. At lower shear stress, the predicted results of these two equations are similar, whereas at higher shear stress, the results of MPM equation are smaller than those of EB equation, and more close to the observed data. For a comparison of three surface-based transport models for mixed-size sediment, the readers are referred to Wilcock and Crowe [2003].

5.2. Full Transport

[33] Two sets of experimental data [Samaga et al., 1986; Sun and Donahue, 2000] and one set of field data from East

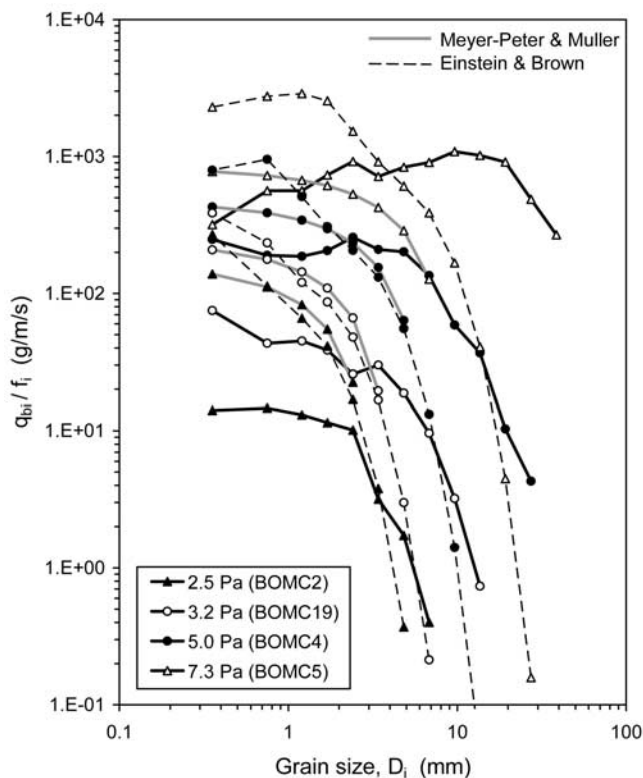


Figure 13. Comparison of observed fractional transport rates with predicted results of two more common bed load formulas for uniform sediment (data from BOMC [Wilcock and McArdell, 1997]).

Fork River [Leopold and Emmett, 1977] were used to test the proposed model for the fully mobilized transport. The data of Samaga *et al.* [1986] include 364 fractional transport rates with high ratios of bed shear stress to critical shear stress (ranging from 3.5 to 10). Four types of sediment were used in their experiments, with D_{50} ranging from 0.20 to 0.35 mm and $\sigma_g < 4$. The experiments of Sun and Donahue [2000] were carried out with four sand/gravel mixtures of grains between 0.04 and 9 mm, with D_{50} ranging from 0.48 to 0.88 mm and $\sigma_g < 3.5$. A total of 9 experimental runs were performed with the equilibrium transport conditions, yielding 112 fractional transport rates. The East Fork River data include 92 fully-mobilized fractional transport rates for grain sizes between 0.3 and 4.8 mm, with τ_0 ranging from 1.7 to 5.4 Pa. Shown in Figure 12b is an overall comparison of the predicted fractional transport rates with the observed ones. As can be seen, the model results are in reasonably good agreement with the measured data. Despite that our model is not developed specifically for the full transport, the results of our model are as good as those of the previous full transport model proposed by Sun and Donahue [2000], with our R^2 value slightly higher than theirs by 1%. Moreover, similar to the results shown earlier for the partial transport, the present model tends to overestimate those extremely low fractional transport rates also for the full transport condition.

6. Application to Mobility Assessment

[34] The partial transport model can be used to assess the fractional mobility of mixed-size sediment under a given flow condition. The need for a simple but reasonably accurate method to evaluate the fractional mobility stems from the fact that the active proportion of each fraction is an important parameter in modeling the partial transport of mixed-size sediment but generally difficult to measure. Point counting of the colored bed is a feasible method in the laboratory but impractical in the field, yet partial transport is recently documented in a natural channel using the magnetically tagged gravels [Haschenburger and Wilcock, 2003]. In this section we apply the proposed model to evaluate the fractional mobility using the currently accessible partial transport data. The assessment results are further used to explore the effect of sand content on the grain mobility.

6.1. Assessment of Fractional Mobility

[35] The fractional transport formula presented in equation (5) provides a simple means to evaluate the fractional mobility. For a transport event, typically given are the fractional transport rate q_{bi} , surface proportion f_{bi} and bed shear stress τ_0 . To use equation (5) for mobility assessment, the long-run moving probability $P_{M,i}$ and mean particle velocity $V_{p,i}$ need to be determined with equations (3) and (11), respectively. In equation (3), the entrainment probability $P_{E,i}$ is evaluated with the cumulative distribution LN(0.240, 0.268) (see section 3.1) and the ratio of mean holding time $R_{T,i}$ is estimated by equation (12), both of which vary as a function of θ'_i . In equation (11), the saltation velocity $V_{S,i}$, rolling velocity $V_{R,i}$, and two weighting coefficients are all varying as a function of θ'_i , as described in section 4.4. With these as the input of equation (5), the only unknown Y_i can be evaluated. To check if the calculated Y_i values agree with the measured results, the BOMC

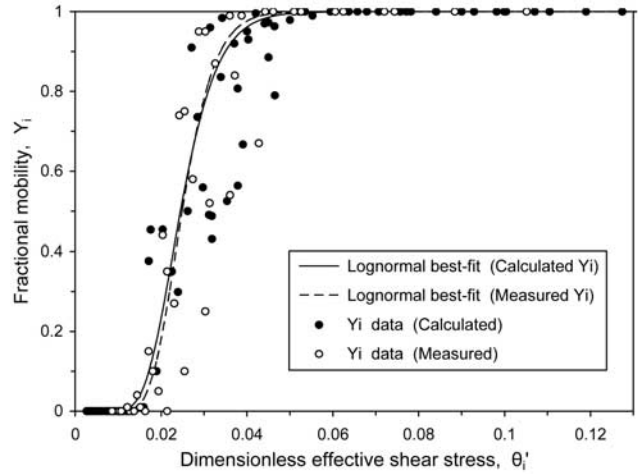


Figure 14. Relation between fractional mobility and dimensionless effective shear stress (BOMC data of Wilcock and McArdell [1997]). The best fit cumulative lognormal curves of the calculated and measured fractional mobility are in good agreement.

data [Wilcock and McArdell, 1997] were used. Figure 14 demonstrates the calculated and measured values of Y_i along with their best fit curves. The calculated results are best fitted by a cumulative lognormal distribution LN(0.0255, 0.0072), with $R^2 = 0.87$, while the measured Y_i values are well represented by LN(0.0257, 0.0062), with $R^2 = 0.82$. The demonstrated agreement between the best fit curves of the calculated and measured results suggests that the fractional mobility evaluated with equation (5) is within the reasonable range and the proposed model may thus be practically applied to the assessment of fractional mobility.

6.2. Effect of Sand Content on Grain Mobility

[36] It has been reported that sand content has a direct effect on the entrainment and transport of gravel-sand mixtures [e.g., Wilcock, 1998; Wilcock and Kenworthy, 2002]. Within a range of sand content $0 < f_s < 0.4$, the entrainment thresholds of the gravel and sand reduce with the increase of f_s . Variations of the entrainment thresholds with f_s for the two-fraction sediment (i.e., gravel and sand) have been intensively studied [e.g., Wilcock and Kenworthy, 2002; Wilcock and Crowe, 2003]. However, the effect of sand content on the mobility of sediment has not yet been fully investigated due to the major difficulty involved in the assessment of fractional mobility. Here we used the proposed model to evaluate the fractional mobility of sediment mixtures containing various proportions of sand; we also explored the variation of grain mobility with f_s . Such a study has been made possible owing to the comprehensive data set recently released by Wilcock *et al.* [2001]. Their data covered a wide range of transport rates for four sediment mixtures containing the following sand proportions (with the sediment name indicated in the parentheses): 6.2% (J06), 14.9% (J14), 20.6% (J21), and 27% (J27). Two additional field data from East Fork River with $f_s = 0.59$ [Leopold and Emmett, 1977] and Goodwin Creek with $f_s = 0.34$ [Kuhnle, 1992] were also included in the analysis to extend the range of f_s . A total of 8 data sets, including our colored bed experimental data with $f_s = 0.3$ (shown in

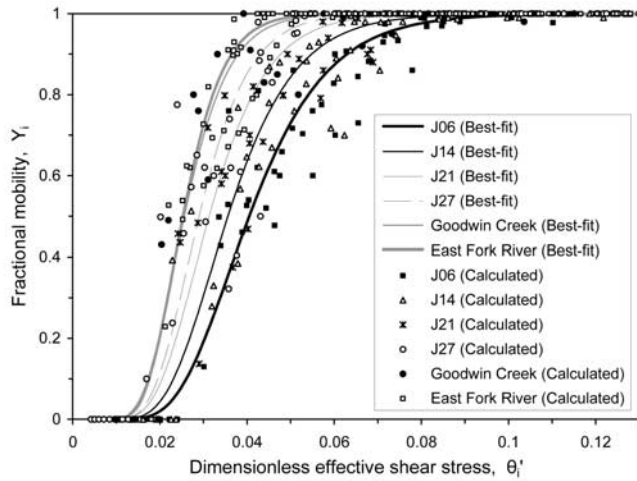


Figure 15. Relation between fractional mobility and dimensionless effective shear stress for data: J06 ~ J27, $f_s = 0.06 \sim 0.27$ [Wilcock *et al.*, 2001]; Goodwin Creek, $f_s = 0.34$ [Kuhnle, 1992]; East Fork River, $f_s = 0.59$ [Leopold and Emmett, 1977].

Figure 6) and BOMC data [Wilcock and McArdell, 1997] with $f_s = 0.34$ (shown in Figure 14) were analyzed. Herein the size boundary between the sand and gravel was taken to be 2 mm as a common standard [Wilcock *et al.*, 2001].

[37] The calculated Y_i values for each data set along with their best fit lognormal curve are demonstrated in Figure 15, with the mean μ_{LN} , standard deviation σ_{LN} , and R^2 values of the cumulative lognormal distributions of all analyzed data sets listed in Table 5. The R^2 values of these best fit curves range from 0.84 to 0.99, implying that considerably consistent results can be obtained with this approach. As revealed in Figure 15, the mobility curves follow a sequence with the corresponding f_s values decreasing from left to right, larger variations with respect to θ'_i can be observed for the curves with smaller f_s values. Such trends are reflected by the variations of μ_{LN} and σ_{LN} , respectively. To demonstrate this, variations of μ_{LN} and σ_{LN} with f_s are shown in Figure 16, where the decreasing trends of μ_{LN} and σ_{LN} are apparent for the range $0.06 \leq f_s \leq 0.34$. Two implications are acquired from such results. First, the reduction of μ_{LN} with f_s indicates that the value of θ'_i corresponding to the same level of Y_i (say 0.5) is smaller for the higher f_s value,

Table 5. Mean, Standard Deviation, and R^2 Values of Best Fit Lognormal Distributions^a

Data	Sand Content f_s	Mean μ_{LN}	Standard Deviation σ_{LN}	R^2
J06	0.06	0.0429	0.0152	0.91
J14	0.15	0.0376	0.0130	0.91
J21	0.21	0.0330	0.0112	0.84
J27	0.27	0.0300	0.0095	0.88
BOMC (Calculated)	0.34	0.0255	0.0072	0.87
C-1 ~ C-7	0.30	0.0287	0.0082	0.89
Goodwin Creek	0.34	0.0269	0.0089	0.99
East Fork River	0.59	0.0263	0.0076	0.89

^aSources of data: J06 ~ BOMC, Wilcock *et al.* [2001]; C-1 ~ C-7, this study; Goodwin Creek, Kuhnle [1992]; East Fork River, Leopold and Emmett [1977].

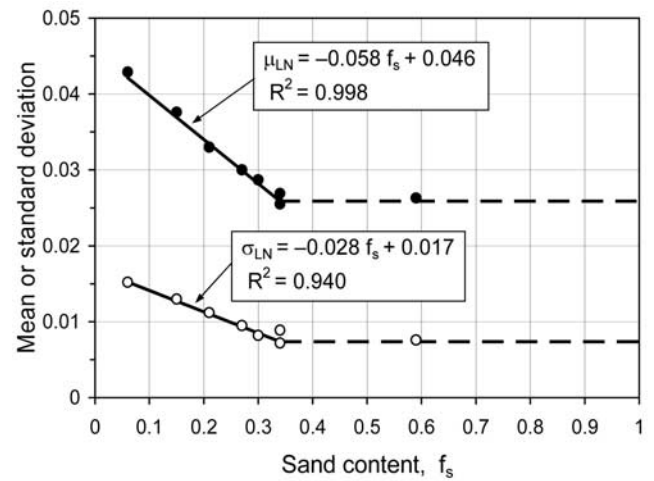


Figure 16. Variations of μ_{LN} and σ_{LN} with sand content f_s , where μ_{LN} and σ_{LN} are mean and standard deviation of the best fit cumulative lognormal distribution for the $Y_i - \theta'_i$ relation.

indicating that sands act to serve as a lubricant in the sediment mixture. The existence of fine-grained sand in the gravel-sand mixture is favorable to the mobilization of sediment grains, which is consistent with the result concerning the variation of entrainment thresholds with f_s . Second, the decrease of σ_{LN} with f_s implies that the range of θ'_i corresponding to partial mobility is narrower for the greater f_s . In other words, for the lower sand content, the condition of partial transport exists over a wider range of flows. For example, Figure 15 reveals that the range of θ'_i corresponding to partial mobility (i.e., $Y_i = 0 \sim 0.99$) for $f_s = 0.06$ (J06), $\theta'_i = 0.01 \sim 0.09$, is twice the range for $f_s = 0.59$ (East Fork River), $\theta'_i = 0.01 \sim 0.05$. In summary, in the presence of more sand grains, the smaller value of μ_{LN} and the narrower band of θ'_i for partial mobility make the condition of full transport easier to achieve, which coincides with the observations that full transport is dominant in most sand bed rivers. Note that both the BOMC and Goodwin Creek data are for a value of $f_s = 0.34$, and that their results of μ_{LN} and σ_{LN} are very similar (as demonstrated in Figure 16), suggesting that the results obtained from the current approach are of reasonable consistency.

[38] Linear variations of μ_{LN} and σ_{LN} with f_s (for $0.06 \leq f_s \leq 0.34$) are expressed as the following (with $R^2 = 0.998$ and 0.940, respectively):

$$\mu_{LN} = -0.058f_s + 0.046 \quad (13a)$$

$$\sigma_{LN} = -0.028f_s + 0.017 \quad (13b)$$

For $f_s > 0.34$, μ_{LN} and σ_{LN} appear to remain constant (see Figure 16), which is based on a single data point of East Fork River and thus needs further confirmation with more data. Nonetheless, the results shown in Figure 16 indicate that sand content has a direct influence on grain mobility within a narrow range of f_s , which is consistent with previous results concerning the effect of sand content on the entrainment thresholds [e.g., Wilcock and Kenworthy, 2002]. For a specified value of f_s , equation (13) can be practically employed to estimate μ_{LN} and σ_{LN} , and then the resulting cumulative lognormal distribution can be used to

evaluate the fractional mobility Y_i corresponding to the given θ'_i value. The results presented herein are useful in two aspects. First, the fractional mobility, a very important parameter of the partial transport model, can be easily determined with the given values of f_s and θ'_i . Second, with the Y_i curve obtained for a given f_s value, the range of θ'_i corresponding to partial mobility can be identified, and the quantitative criteria for distinguishing partial transport from full transport can be established.

7. Summary and Conclusions

[39] In this paper we present a stochastic framework for modeling partial transport of mixed-size sediment. The proposed relation, as given by (5), predicts the fractional transport rate with the long-run moving probability, mean particle velocity, and fractional mobility, all of which vary as a function of the dimensionless effective shear stress θ'_i . The movement of bed load particles, which is viewed as a random combination of single-step static and moving states, is described by a restructured pseudo four-state continuous-time Markov process. For a continuous-time Markov process, the long-run probability of a bed load particle being in the moving state can be evaluated with the instantaneous entrainment probability and ratio of mean single-step holding time. Herein we adopt a most updated version of entrainment probability that takes into account the rolling and lifting modes of incipient motion and a ratio of mean holding time derived from the present experimental study.

[40] To determine the model parameters, two types of experiments were performed in this study. The first was carried out with the colored bed to observe the fractional mobility and partial bed load transport. The second was conducted with the plain bed to observe the single-step bed load motions and mean particle velocity. The results reveal that the fractional mobility can be approximated by a cumulative lognormal distribution of θ'_i , with its mean and standard deviation affected by the sand content of the sediment mixtures. Given the rolling and lifting probabilities for sediment entrainment, the mean particle velocity can be determined with the weighted average of the rolling and saltation velocities. The results also reveal that the single-step holding time in the moving state is much shorter than that in the static state, both are well fitted by the exponential distributions, which justifies the underlying assumption of the continuous-time Markov process. On the basis of the experimental results, we present in this paper a first physically based relation that predicts the ratio of mean holding time with θ'_i .

[41] The proposed model was tested with the field and laboratory data pertaining to both partial and full transport conditions. The model results are in good agreement with the partial transport data, and also coincide well with the full transport data. The model was then applied to assess the fractional mobility of mixed-size sediment. A variety of laboratory and field data covering a wide range of flows and sediments were used to explore the effect of sand content on the fractional mobility. The relationship between the calculated Y_i values and θ'_i is well fitted by the cumulative lognormal distributions, with the values of mean μ_{LN} and standard deviation σ_{LN} linearly decreasing with f_s for $f_s < 0.34$. The results imply that sands act to serve as a lubricant in the sediment mixture. The presence of fine-grained sand

in the gravel-sand mixture is beneficial to the mobilization of sediment particles. At higher f_s , the condition of partial transport exists within a narrower range of flows. The results reveal that the range of θ'_i corresponding to partial mobility for $f_s = 0.06$ is approximately twice that for $f_s = 0.34$. The condition of full transport is easier to achieve in the presence of more sand, which explains the dominance of the full transport condition in most sand bed rivers. However, for $f_s > 0.34$, the single data appear to indicate that the values of μ_{LN} and σ_{LN} remain constant, implying that sand content has a direct influence on grain mobility within a narrow range of f_s , which is consistent with the previous results regarding the effect of sand content on the threshold shear stress for sediment entrainment. In this paper we present results that can be practically employed to determine the fractional mobility, which is an important parameter of the partial transport model but conventionally hard to obtain. We also provide results that can be applied to establish the quantitative criteria for distinguishing partial transport from full transport, which may well be useful to river managers in sustaining the riverine environments and natural resources.

[42] In this study we explore the effect of sand content on fractional mobility, thus provide new insights into the process of partial transport. However, some of the model components can be refined in future studies. These include the incorporation of turbulent bursting in the formulation of entrainment probability, modification of the subsurface entrainment correction factor to include the effects of vertical sorting and exchange depth, correction of the hiding factor for the fully mobilized finest size fractions, collection of more data to extend the valid ranges of the proposed rolling velocity and ratio of mean holding time, among others. Some of these tasks are currently undertaken by the authors. In addition, the complexities of natural gravel bed rivers, such as the spatial and temporal variations of bed shear stress, sand content, and thus the bed load transport rate must be incorporated into a routing algorithm applicable to the problems involving grain sorting between the transport and the bed or size-dependent dispersion of sediment through a river system.

Appendix A: Derivation of Limiting Probability

[43] The derivation presented below is for the grains of fraction i , denoted by a subscript. Given $P_{E,i}$ is the instantaneous entrainment probability of a bed load particle, the probability of a transition to the moving state at a single-step point can be taken as $P_{E,i}$, and the probability of a transition to the static state at a single-step point is taken to be $(1 - P_{E,i})$. In the context of a 'pseudo four-state' continuous-time Markov process, the matrix of instantaneous transition probability can be expressed as

$$\mathbf{P} = [P_{mn,i}] = \begin{bmatrix} 0 & P_{E,i} & 1 - P_{E,i} & 0 \\ 1 - P_{E,i} & 0 & 0 & P_{E,i} \\ 1 - P_{E,i} & P_{E,i} & 0 & 0 \\ 1 - P_{E,i} & P_{E,i} & 0 & 0 \end{bmatrix} \quad (\text{A1})$$

where $P_{mn,i}$ is transition probability from state m to n at a single-step point, for $m, n = 1, \dots, 4$. If the single-step

holding time in state m follows the exponential distribution with a mean value $T_{m,i} (=1/v_{m,i})$, where $v_{m,i}$ = mean transition rate in state m , then the transition probability from state m to n within a time period t , denoted as $P_{mn,i}(t)$, satisfies Kolmogorov differential equations, i.e.,

$$\frac{d\mathbf{P}(t)}{dt} = \mathbf{P}'(t) = \mathbf{P}(t)\mathbf{G} \quad (\text{A2})$$

where $\mathbf{P}(t)$ = matrix form of $P_{mn,i}(t)$; \mathbf{G} = generator matrix, which is given by

$$\mathbf{G} = [g_{mn,i}] = \begin{bmatrix} -v_{1,i} & v_{1,i}P_{E,i} & v_{1,i}(1-P_{E,i}) & 0 \\ v_{2,i}(1-P_{E,i}) & -v_{2,i} & 0 & v_{2,i}P_{E,i} \\ v_{3,i}(1-P_{E,i}) & v_{3,i}P_{E,i} & -v_{3,i} & 0 \\ v_{4,i}(1-P_{E,i}) & v_{4,i}P_{E,i} & 0 & -v_{4,i} \end{bmatrix} \quad (\text{A3})$$

where $g_{mn,i}$ = transition rate from state m to $n = v_{m,i}P_{mn,i}$ for $m \neq n$, and $g_{mm,i} = -v_{m,i}$. According to the Markov theorem, there exists a long-run limiting probability, denoted as $P_{n,i}$, such that the probability of being in state n at large t is independent of the initial state m , i.e.,

$$P_{n,i} = \lim_{t \rightarrow \infty} P_{mn,i}(t) \quad (\text{A4})$$

Because the limiting probability is not a function of t , equation (A2) can be rewritten as

$$\lim_{t \rightarrow \infty} \mathbf{P}'(t) = 0 = \mathbf{G}^T \mathbf{P}_\infty \quad (\text{A5})$$

where \mathbf{G}^T = transpose matrix of \mathbf{G} ; \mathbf{P}_∞ = column vector of limiting probability. The solution of equation (A5) is

$$\mathbf{P}_\infty = \begin{bmatrix} P_{1,i} \\ P_{2,i} \\ P_{3,i} \\ P_{4,i} \end{bmatrix} = \frac{1}{R} \begin{bmatrix} r_{1,i} \\ r_{2,i} \\ r_{3,i} \\ r_{4,i} \end{bmatrix} = \frac{1}{R} \begin{bmatrix} v_{1,i}P_{E,i}(2-P_{E,i})/v_{2,i}(1-P_{E,i}) \\ v_{1,i}(1-P_{E,i})/v_{3,i} \\ v_{1,i}P_{E,i}^2(2-P_{E,i})/v_{4,i}(1-P_{E,i}) \end{bmatrix} \quad (\text{A6})$$

where

$$R = \sum_{n=1}^4 r_{n,i}$$

Since states 1 and 3 are both static, states 2 and 4 are both moving, it is known that $v_{1,i} = v_{3,i} = 1/T_{S,i}$ and $v_{2,i} = v_{4,i} = 1/T_{M,i}$. The long-run probability for a bed load particle being in the moving state is obtained by summing up $P_{2,i}$ and $P_{4,i}$, i.e., $P_{M,i} = P_{2,i} + P_{4,i}$, leading to (3). Similarly, the limiting probability in the static state is evaluated by $P_{S,i} = P_{1,i} + P_{3,i}$. It is noted that the form of equation (3) is identical to the result obtained by *Sun and Donahue* [2000], although

the discrete-time Markovian transition probabilities were erroneously used in their continuous-time two-state model. However, we have mathematically shown that the continuous-time Markov process is a limiting case of the discrete-time Markov process, thus the limiting probabilities obtained by *Sun and Donahue* [2000] necessarily coincide with our rigorously derived results.

Notation

D_i	grain diameter of fraction i .
D_m	mean grain size.
D_{50}	median grain size.
D_{65}	grain size for which 65% is finer.
e	base of natural logarithms (≈ 2.718).
f_i	proportion of fraction i on the bed.
f_s	sand content (\approx proportion of sand in the bed).
\mathbf{G}	generator matrix.
g	gravitational acceleration.
$g_{mn,i}$	transition rate from state m to n .
h	flow depth.
i	fraction i , denoted by a subscript.
L_i	mean single step length.
m_i	mass of a grain.
N_i	number of active grains per unit area.
$P_{E,i}$	instantaneous entrainment probability = $P_{R,i} + P_{L,i}$.
$P_{L,i}$	lifting probability.
$P_{M,i}$	long-run moving probability.
$P_{R,i}$	rolling probability.
$P_{mn,i}$	instantaneous transition probability from state m to n .
$P_{mn,i}(t)$	transition probability from state m to n within a time interval t .
$P_{n,i}$	long-run limiting probability of being in state n at large t .
\mathbf{P}	matrix of instantaneous transition probability.
\mathbf{P}_∞	column vector of limiting probability.
$\mathbf{P}(t)$	matrix form of $P_{mn,i}(t)$.
p_i	proportion of fraction i in bed load.
q_b	total bed load transport rate, g/m/s.
$q_{b,i}$	fractional transport rate ($=q_b p_i$), g/m/s.
R^2	coefficient of determination.
$R_{T,i}$	ratio of mean holding time = $T_{S,i}/T_{M,i} = v_{M,i}/v_{S,i}$.
$T_{M,i}$	mean single-step holding time in the moving state.
$T_{S,i}$	mean single-step holding time in the static state.
$T_{m,i}$	mean single-step holding time in state m .
U	mean velocity.
u_*	shear velocity.
$V_{R,i}$	dimensionless rolling velocity.
$V_{S,i}$	dimensionless saltation velocity.
$V_{P,i}$	dimensionless mean particle velocity.
$v_{m,i}$	mean transition rate in state m .
Y_i	mobility of size fraction i .
Y_i^*	relative mobility of fraction $i = Y_i/\bar{Y}$.
\bar{Y}	mean mobility of sediment.
z_0	bed roughness length.
Δ_i	subsurface entrainment correction factor.
γ	specific weight of water.
γ_s	specific weight of sediment.
θ_i	dimensionless shear stress based on D_i .

θ'_i	dimensionless effective shear stress based on $D_i (= \xi_i \theta_i)$.
ρ	density of water.
ρ_s	density of sediment.
ξ_i	hiding factor of fraction i .
μ_{LN}	mean of best fit cumulative lognormal distribution.
σ_g	geometric standard deviation of grain size distribution.
σ_{LN}	standard deviation of best fit cumulative lognormal distribution.
τ_0	bed shear stress.
κ	von Karman constant.

[44] **Acknowledgments.** This research was supported with the Young Investigator Grant of National Science Council, Republic of China. Y. C. Lin and Y. C. Shen assisted in setting up and carrying out the flume experiments. The authors acknowledge P. R. Wilcock for releasing his comprehensive data set as an AGU electronic supplement. Comments from two anonymous reviewers helped improve the paper.

References

- Abbott, J. E., and J. R. D. Francis (1977), Saltation and suspension trajectories of solid grains in a water stream, *Philos. Trans. R. Soc. London, Ser. A*, 284, 225–254.
- Armanini, A. (1995), Non-uniform sediment transport: Dynamics of the active layer, *J. Hydrol. Res.*, 33, 611–622.
- Bridge, J. S., and S. J. Bennett (1992), A model for the entrainment and transport of sediment grains of mixed sizes, shapes, and densities, *Water Resour. Res.*, 28, 337–363.
- Bridge, J. S., and D. F. Dominic (1984), Bed load grain velocities and sediment transport rates, *Water Resour. Res.*, 20, 476–490.
- Cheng, N.-S., and Y.-M. Chiew (1998), Pickup probability for sediment entrainment, *J. Hydraul. Eng.*, 124, 232–235.
- Drake, T. G., R. L. Shreve, W. E. Dietrich, P. J. Whiting, and L. B. Leopold (1988), Bedload transport of fine gravel observed by motion-picture photography, *J. Fluid Mech.*, 192, 193–217.
- Einstein, H. A. (1937), Bed load transport as a probability problem, Ph.D. thesis, Fed. Inst. of Technol., Zurich, Switzerland.
- Einstein, H. A. (1942), Formula for the transportation of bed load, *Trans. ASCE*, 107, 561–597.
- Einstein, H. A. (1950), The bed load function for sediment transportation in open channel flows, *Tech. Bull. U.S. Dep. Agric.*, 1026.
- Francis, J. R. D. (1973), Experiments on the motion of solitary grains along the bed of water stream, *Proc. R. Soc. London, Ser. A*, 332, 443–471.
- Gordon, R., J. B. Carmichael, and F. J. Isackson (1972), Saltation of plastic balls in a one-dimensional flume, *Water Resour. Res.*, 8, 444–459.
- Haschenburger, J. K., and P. R. Wilcock (2003), Partial transport in a natural gravel bed channel, *Water Resour. Res.*, 39(1), 1020, doi:10.1029/2002WR001532.
- Hirano, M. (1971), River bed degradation with armoring, *Proc. Jpn. Soc. Civ. Eng.*, 195, 55–65.
- Hoey, T. B., and R. Ferguson (1994), Numerical simulation of downstream fining by selective transport in gravel bed rivers: Model development and illustration, *Water Resour. Res.*, 30, 2251–2260.
- Hubbell, D. W., and W. W. Sayre (1964), Sand transport studies with radioactive tracers, *J. Hydraul. Div. Am. Soc. Civ. Eng.*, 90(HY3), 39–68.
- Julien, P. Y. (1998), *Erosion and Sedimentation*, Cambridge Univ. Press, New York.
- Kuhnle, R. A. (1992), Fractional transport rates of bedload on Goodwin Creek, in *Dynamics of Gravel-Bed Rivers*, edited by P. Billi et al., pp. 141–155, John Wiley, Hoboken, N. J.
- Lee, H. Y., and I. S. Hsu (1994), Investigation of saltating particle motions, *J. Hydraul. Eng.*, 120, 831–845.
- Lee, H. Y., J. Y. You, and Y. T. Lin (2002), Continuous saltating process of multiple sediment particles, *J. Hydraul. Eng.*, 128, 443–450.
- Leopold, L. B., and W. W. Emmett (1977), 1976 bedload measurements, East Fork River, Wyoming, *Proc. Natl. Acad. Sci. U. S. A.*, 74(7), 2644–2648.
- Luque, R. F., and R. van Beek (1976), Erosion and transport of bed-load sediment, *J. Hydraul. Res.*, 14, 127–144.
- Misri, R. L., R. J. Garde, and K. G. Ranga Raju (1984), Bed load transport of coarse nonuniform sediments, *J. Hydraul. Eng.*, 110, 312–323.
- Nelson, B. L. (1995), *Stochastic Modeling: Analysis and Simulation*, McGraw-Hill, New York.
- Niño, Y., and M. García (1998), Experiments on saltation of sand in water, *J. Hydraul. Eng.*, 124, 1014–1025.
- Niño, Y., M. García, and L. Ayala (1994), Gravel saltation: I. Experiments, *Water Resour. Res.*, 30, 1907–1914.
- Paintal, A. S. (1971), A stochastic model of bed-load transport, *J. Hydraul. Res.*, 9, 527–554.
- Paola, C., G. Parker, R. Seal, S. K. Sinha, J. B. Southard, and P. R. Wilcock (1992), Downstream fining by selective deposition in a laboratory flume, *Science*, 258, 1757–1760.
- Parker, G., and A. J. Sutherland (1990), Fluvial armor, *J. Hydraul. Res.*, 28, 529–544.
- Parker, G., C. Paola, and S. Leclair (2000), Probabilistic Exner sediment continuity equation for mixtures with no active layer, *J. Hydraul. Eng.*, 126, 818–826.
- Proffitt, G. T., and A. J. Sutherland (1983), Transport of non-uniform sediments, *J. Hydraul. Res.*, 21, 33–43.
- Ross, S. M. (2000), *An Introduction to Probability Models*, Academic, San Diego, Calif.
- Samaga, B. R., K. G. Ranga Raju, and R. J. Garde (1986), Bed load transport of sediment mixtures, *J. Hydraul. Eng.*, 112, 1003–1018.
- Sekine, M., and H. Kikkawa (1992), Mechanics of saltating grains. II, *J. Hydraul. Eng.*, 118, 536–558.
- Shvidchenko, A. B., G. Pender, and T. B. Hoey (2001), Critical shear stress for incipient motion of sand/gravel streambeds, *Water Resour. Res.*, 37, 2273–2283.
- Sun, Z., and J. Donahue (2000), Statistically derived bedload formula for any fraction of nonuniform sediment, *J. Hydraul. Eng.*, 126, 105–111.
- Wiberg, P. L., and J. D. Smith (1985), A theoretical model for saltating grains in water, *J. Geophys. Res.*, 90(C4), 7341–7354.
- Wilcock, P. R. (1996), Estimating local bed shear stress from velocity observations, *Water Resour. Res.*, 32, 3361–3366.
- Wilcock, P. R. (1997), The components of fractional transport rate, *Water Resour. Res.*, 33, 247–258.
- Wilcock, P. R. (1998), Two-fraction model of initial sediment motion in gravel-bed rivers, *Science*, 280, 410–412.
- Wilcock, P. R., and J. C. Crowe (2003), Surface-based transport model for mixed-size sediment, *J. Hydraul. Eng.*, 129, 120–128.
- Wilcock, P. R., and S. T. Kenworthy (2002), A two-fraction model for the transport of sand/gravel mixtures, *Water Resour. Res.*, 38(10), 1194, doi:10.1029/2001WR000684.
- Wilcock, P. R., and B. W. McArdeil (1993), Surface-based fractional transport rates: Mobilization thresholds and partial transport of a sand-gravel sediment, *Water Resour. Res.*, 29, 1297–1312.
- Wilcock, P. R., and B. W. McArdeil (1997), Partial transport of a sand/gravel sediment, *Water Resour. Res.*, 33, 235–245.
- Wilcock, P. R., S. T. Kenworthy, and J. C. Crowe (2001), Experimental study of the transport of mixed sand and gravel, *Water Resour. Res.*, 37, 3349–3358.
- Wu, F.-C. (2000), Modeling embryo survival affected by sediment deposition into salmonid spawning gravels: Application to flushing flow prescriptions, *Water Resour. Res.*, 36, 1595–1603.
- Wu, F.-C., and Y.-J. Chou (2003a), Rolling and lifting probabilities for sediment entrainment, *J. Hydraul. Eng.*, 129, 110–119.
- Wu, F.-C., and Y.-J. Chou (2003b), Simulation of gravel-sand bed response to flushing flows using a two-fraction entrainment approach: Model development and flume experiment, *Water Resour. Res.*, 39(8), 1211, doi:10.1029/2003WR002184.
- Wu, F.-C., and Y.-C. Lin (2002), Pickup probability of sediment under log-normal velocity distribution, *J. Hydraul. Eng.*, 128, 438–442.
- Wu, F.-C., and C.-K. Wang (1998), Higher-order approximation techniques for estimating stochastic parameter of a sediment transport model, *Stochastic Hydrol. Hydraul.*, 12, 359–375.
- Wu, W., S. S. Y. Wang, and Y. Jia (2000), Nonuniform sediment transport in alluvial rivers, *J. Hydraul. Res.*, 38, 427–434.

F.-C. Wu and K.-H. Yang, Department of Bioenvironmental Systems Engineering, National Taiwan University, Taipei 106, Taiwan. (fcwu@hy.ntu.edu.tw)